



**HAL**  
open science

## New sensitive tools to characterize meta-metabolome response to short- and long-term cobalt exposure in dynamic river biofilm communities

Simon Colas, Benjamin Marie, Soizic Morin, Mathieu Milhe-Poutingon, Pierre Foucault, Siann Chalvin, Clémentine Gelber, Patrick Baldoni-Andrey, Nicholas GuriEFF, Claude Fortin, et al.

### ► To cite this version:

Simon Colas, Benjamin Marie, Soizic Morin, Mathieu Milhe-Poutingon, Pierre Foucault, et al.. New sensitive tools to characterize meta-metabolome response to short- and long-term cobalt exposure in dynamic river biofilm communities. *Science of the Total Environment*, 2024, 927, pp.171851. 10.1016/j.scitotenv.2024.171851 . hal-04554625

**HAL Id: hal-04554625**

**<https://univ-pau.hal.science/hal-04554625>**

Submitted on 22 Apr 2024

**HAL** is a multi-disciplinary open access archive for the deposit and dissemination of scientific research documents, whether they are published or not. The documents may come from teaching and research institutions in France or abroad, or from public or private research centers.

L'archive ouverte pluridisciplinaire **HAL**, est destinée au dépôt et à la diffusion de documents scientifiques de niveau recherche, publiés ou non, émanant des établissements d'enseignement et de recherche français ou étrangers, des laboratoires publics ou privés.



Distributed under a Creative Commons Attribution - NonCommercial 4.0 International License



## New sensitive tools to characterize meta-metabolome response to short- and long-term cobalt exposure in dynamic river biofilm communities

Simon Colas<sup>a,\*</sup>, Benjamin Marie<sup>b</sup>, Soizic Morin<sup>c</sup>, Mathieu Milhe-Poutingon<sup>a</sup>, Pierre Foucault<sup>b,d</sup>, Siann Chalvin<sup>a</sup>, Clémentine Gelber<sup>e</sup>, Patrick Baldoni-Andrey<sup>e</sup>, Nicholas GuriEFF<sup>f</sup>, Claude Fortin<sup>g</sup>, Séverine Le Faucheur<sup>a</sup>

<sup>a</sup> Université de Pau et des Pays de l'Adour, E2S-UPPA, CNRS, IPREM, Pau, France

<sup>b</sup> UMR 7245 CNRS/MNHN "Molécules de Communication et Adaptation des Micro-organismes", Muséum National d'Histoire Naturelle, Paris, France

<sup>c</sup> INRAE UR EABX, Cestas, France

<sup>d</sup> UMR7618 iEES-Paris, Sorbonne Université, Paris, France

<sup>e</sup> TotalEnergies, Pole d'Etudes de Recherche de Lacq, France

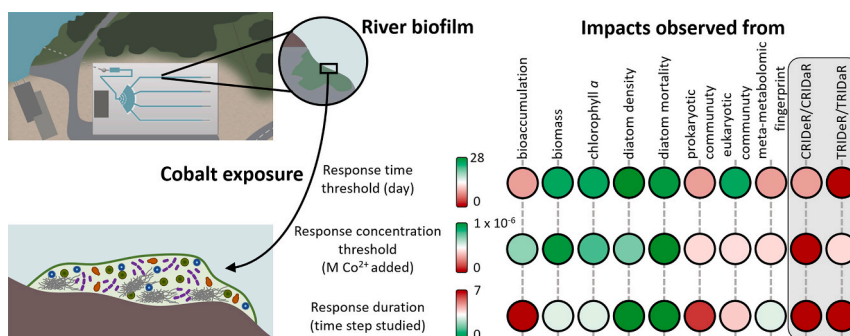
<sup>f</sup> Rio Tinto, Closure R&D, Brisbane, Queensland, Australia

<sup>g</sup> Institut National de la Recherche Scientifique – Eau Terre Environnement, Québec, Canada

### HIGHLIGHTS

- Prokaryotic community structures were impacted after 1 h of exposure to Co.
- Biofilm meta-metabolome was impacted after 36 s of exposure to Co.
- Biofilm meta-metabolome response was faster than changes in biofilm communities.
- Short- and long-term exposed biofilms have similar CRIDeR initiation thresholds.
- Long-term exposed biofilms have higher CRIDaR initiation thresholds.

### GRAPHICAL ABSTRACT



### ARTICLE INFO

Editor: Yi Yang

#### Keywords:

Microbial ecotoxicity

Multi-omics

Metal

Metabolomics

### ABSTRACT

Untargeted metabolomics is a non-*a priori* analysis of biomolecules that characterizes the metabolome variations induced by short- and long-term exposures to stressors. Even if the metabolite annotation remains lacunar due to database gaps, the global metabolomic fingerprint allows for trend analyses of dose-response curves for hundreds of cellular metabolites. Analysis of dose/time-response curve trends (biphasic or monotonic) of untargeted metabolomic features would thus allow the use of all the chemical signals obtained in order to determine stress levels (defense or damage) in organisms. To develop this approach in a context of time-dependent microbial

**Abbreviations:** AICc, second-order Akaike's information criterion; BMD, benchmark-dose; BMT, benchmark-time; CA, cellulose acetate; CRIDaR, concentration range inducing damage responses; CRIDeR, concentration range inducing defense responses; DOC, dissolved organic carbon; ECDF, empirical cumulative density function; LC-HRMS, liquid chromatography-high resolution mass spectrometry; MOTa, multivariate omics trajectory analysis; PCoA, principal coordinate analysis; PP, polypropylene; TRIDaR, time range inducing damage responses; TRIDeR, time range inducing defense responses.

\* Corresponding author.

E-mail address: [simon.colas@univ-pau.fr](mailto:simon.colas@univ-pau.fr) (S. Colas).

<https://doi.org/10.1016/j.scitotenv.2024.171851>

Received 18 November 2023; Received in revised form 18 March 2024; Accepted 19 March 2024

Available online 20 March 2024

0048-9697/© 2024 The Authors. Published by Elsevier B.V. This is an open access article under the CC BY-NC license (<http://creativecommons.org/licenses/by-nc/4.0/>).

Prokaryotic diversity  
Eukaryotic diversity

community changes, mature river biofilms were exposed for 1 month to four cobalt (Co) concentrations (from background concentration to  $1 \times 10^{-6}$  M) in an open system of artificial streams. The meta-metabolomic response of biofilms was compared against a multitude of biological parameters (including bioaccumulation, biomass, chlorophyll *a* content, composition and structure of prokaryotic and eukaryotic communities) monitored at set exposure times (from 1 h to 28 d). Cobalt exposure induced extremely rapid responses of the meta-metabolome, with time range inducing defense responses (TRIDeR) of around 10 s, and time range inducing damage responses (TRIDaR) of several hours. Even in biofilms whose structure had been altered by Co bioaccumulation (reduced biomass, chlorophyll *a* contents and changes in the composition and diversity of prokaryotic and eukaryotic communities), concentration range inducing defense responses (CRIDeR) with similar initiation thresholds ( $1.41 \pm 0.77 \times 10^{-10}$  M  $\text{Co}^{2+}$  added in the exposure medium) were set up at the meta-metabolome level at every time point. In contrast, the concentration range inducing damage responses (CRIDaR) initiation thresholds increased by 10 times in long-term Co exposed biofilms. The present study demonstrates that defense and damage responses of biofilm meta-metabolome exposed to Co are rapidly and sustainably impacted, even within tolerant and resistant microbial communities.

## 1. Introduction

The current global transition towards decarbonized energy sources has led to the intensification of metal extraction. For example, cobalt (Co) mining has almost doubled since 2010, mostly due to its wide use in electric batteries (U.S. Geological Survey, 2010, 2023). As a consequence, increases in Co levels above background concentrations ( $< 10$  nM) have been reported in aquatic ecosystems surrounding mining areas and industrial sites, up to  $1.9 \times 10^{-5}$  M and  $4.8 \times 10^{-5}$  M respectively (Gray and Eppinger, 2012; Barrio-Parra et al., 2018). The European Chemicals Agency (ECHA) has determined the Predicted No Effect Concentration (PNEC) of Co to be  $1.8 \times 10^{-8}$  M in freshwater (European Chemicals Agency, 2023), while the median hazardous concentration values of 5 % based on a species sensitivity distribution for freshwater organisms have been set at  $3.1 \times 10^{-8}$  M for chronic toxicity using  $\text{EC}_{10}$  values and  $1.2 \times 10^{-7}$  M using  $\text{EC}_{20}$  values (Stubblefield et al., 2020). This metal is an essential trace element of biomolecules involved in the metabolic pathways of various cellular processes (e.g., vitamin B12; Martens et al., 2002). Nevertheless, experiments performed with model organisms, such as microalgae, demonstrated its toxic effects at  $\mu\text{M}$  concentrations on growth (Karthikeyan et al., 2019), lipid peroxidation (Li et al., 2007), pigment contents and photosynthetic activity (El-Sheekh et al., 2003; Plekhanov and Chemeris, 2003; Fawzy et al., 2020).

In rivers, benthic microalgae grow within biofilms, which are communities composed of various types of organisms (i.e., algae, bacteria, fungi and meiofauna). They colonize various submerged substrata within aquatic systems and constitute the basis of the aquatic food web as primary producers. Biofilms are also well-known to accumulate metals as a function of their respective ambient concentration and speciation (Meylan et al., 2003; Lavoie et al., 2012a; Laderriere et al., 2020). Metals can then induce numerous effects at all levels of biological organization, from subcellular (Barranguet et al., 2003; Bonet et al., 2013), cellular (Morin et al., 2008a; Duong et al., 2010; Lavoie et al., 2012b; Morin et al., 2017) through to community (Barranguet et al., 2003; Bonet et al., 2013; Doose et al., 2021). However, to date, very few studies have focused on the effects of Co on either river (Tlili et al., 2011a) or intertidal biofilms (Dutta et al., 2022).

Among the various toxicological effects to biofilms that can be monitored, dysregulation of metabolite composition has been observed to be correlated with contaminant concentration and linked to stresses (Gauthier et al., 2020). Nevertheless, the study of such meta-metabolomic (metabolomics at the community level) responses from biofilms following a stress exposure (including anthropogenic pressures) remains a promising approach, despite its recent emergence (Booth et al., 2011; Gauthier et al., 2020). To this end, characterization of the whole meta-metabolome (*endo*- and *exo*-metabolome; i.e. metabolites contained in organisms and sorbed to their surface, and metabolites excreted outside the organisms) using untargeted Liquid Chromatography-High Resolution Mass Spectrometry (LC-HRMS) would allow for a robust characterization of the meta-metabolomic

fingerprint without requiring an *a priori* selection on the form and function of molecules being analyzed. Monitoring the (meta-)metabolome has the advantage of obtaining an instantaneous snapshot of the state of the organism(s) (Peng et al., 2015). Metabolomic fingerprinting makes it possible to characterize the physiology of organisms according to their ecology and their response to anthropogenic pressures. However, due to gaps in current molecular databases, metabolite annotation levels remain still very limited (da Silva et al., 2015) and concern around 5 % of the whole metabolomic fingerprint signal (Dias et al., 2016). Consequently, 95 % of the metabolomic response information is typically not considered.

A recent meta-analysis demonstrated that the trends of dose-response model curves for biomarkers depend on their biological functions. As such, based on 2595 observations made on 18 phyla exposed to inorganic or organic contaminants, cellular defense responses have been shown to have predominantly biphasic trends, while damage responses have been found to have mostly monotonic trends (Colas and Le Faucheur, 2024). For example, in the case of oxidative stress, it is commonly observed that defense biomarkers (i.e. antioxidant enzymes such as catalase or superoxide dismutase) show biphasic dose-response trends (Bártová et al., 2011; Cheng et al., 2016). And that damage biomarkers (i.e. malondialdehyde) are initiated once defense mechanisms have been overwhelmed (Sonmez et al., 2023), resulting in monotonic dose-response trends (Li et al., 2006; Çelekli et al., 2013). Similar observations were also reported concerning the time-response model curves of defense and damage biomarkers. For example, biphasic trends were observed in the activity of antioxidant enzymes (catalase, superoxide dismutase and glutathione peroxidase) and metallothioneins over time in organisms exposed to metals (Xu et al., 2018; Liu et al., 2019). In contrast, trends for biomarkers of damage such as malondialdehyde and DNA damage were exclusively monotonic over the same period.

In the present study, we aimed to evaluate the use of dose-response curve trends of untargeted meta-metabolomic features to determine stress level in microbial communities exposed to Co. Our hypothesis, based on the results of the aforementioned meta-analysis (Colas and Le Faucheur, 2024), is that it is possible to distinguish two different concentration ranges according to the dose-response curve trends (biphasic vs. monotonic) of the untargeted meta-metabolomic features: a concentration range inducing defense responses (CRIDeR) and a concentration range inducing damage responses (CRIDaR). Based on the same assumption and on the observation of similar trends considering exposure time (for a given concentration), it is also possible to determine from the time-response curve trends of untargeted meta-metabolomic features a time range inducing defense responses (TRIDeR) and a time range inducing damage responses (TRIDaR). To that end, mature river biofilms were exposed to four Co concentrations (background concentration,  $1 \times 10^{-7}$ ,  $5 \times 10^{-7}$  and  $1 \times 10^{-6}$  M) in artificial rivers for 28 days. The bioaccumulation and chronic effects of Co on traditional biological parameters (biomass, chlorophyll *a* contents and diatom density, mortality, and characterization of the prokaryotic and

eukaryotic communities) and the meta-metabolome were monitored at set sampling time points (hour 1, days 1, 3, 7, 14, 21 and 28). The results of traditional biological parameters were compared with CRiDeR/CRiDaR and TRiDeR/TRiDaR determined from dose/time-response curve trends of untargeted meta-metabolomic features. Thus, the complete meta-metabolome analysis of biofilms based on dose/time response curve trends following chronic contaminant exposure could be an innovative and holistic approach to characterize the risk assessment of contaminants in ecosystems.

## 2. Material and methods

### 2.1. Biofilm colonization and exposure to Co in artificial streams

The experiment was carried out from September 15 to November 09, 2021, at the outdoor TotalEnergies facility (pilot rivers) in Lacq (PERL, France) (Fig. S1; Cailleaud et al., 2019). Mature biofilms were naturally colonized on glass slides (10 × 20 cm) in plastic boxes (eight slides per box) for a period of 4-weeks after being placed in the nursery of an open circuit supplied by the *Gave de Pau* river (Tien et al., 2009). Twelve streams (length, 40 m; width, 0.5 m; depth, 0.5 m; flow rate, 7.5 m<sup>3</sup>·h<sup>-1</sup>) were randomly assigned a Co exposure concentration, with a total of three replicate streams for each of the four exposure conditions (background concentration in the *Gave de Pau* used as the control, 1 × 10<sup>-7</sup>, 5 × 10<sup>-7</sup> and 1 × 10<sup>-6</sup> M).

Co (Cobalt(II) chloride hexahydrate, 98 %, Thermo Scientific Chemicals) solutions of 1.09 × 10<sup>-2</sup>, 5.43 × 10<sup>-2</sup> and 1.09 × 10<sup>-1</sup> M were added to streams one day prior to beginning exposures (day 0) to obtain stabilized nominal Co concentrations of 1 × 10<sup>-7</sup>, 5 × 10<sup>-7</sup> and 1 × 10<sup>-6</sup> M. Cobalt solutions were injected continuously (71 mL·h<sup>-1</sup>) by a piston pump and mechanically dispersed in the water by shearing valves (Netzsch, Nemo, Germany) throughout the experiment. At the commencement of exposures, an open box containing mature biofilm slides was placed in each stream, 15 m downstream of the injection pump. The upstream nursery constituted of a reservoir containing living organisms, allowing for the promotion of natural and continuous colonization within the streams during the 28 days of experimentation. One biofilm slide from each stream was collected at set time points (1 h; 1, 3, 7, 14, 21 and 28 d). Subsamples from every slide were taken to determine total biofilm Co content, intracellular biofilm Co content, chlorophyll *a* content, meta-metabolome, prokaryotic and eukaryotic community characterization, and diatom populations. Lugol solution (Sigma-Aldrich, Germany) was added to each sample for diatom population monitoring (final concentration of 0.01 % Lugol), which were then stored in the dark at 4 °C. Collected biofilms to be analyzed for Co intracellular accumulation were placed in the dark at 4 °C until treatment up to 3 h (see Section 2.3). Other samples were stored in the dark at -20 °C before lyophilization and further analyses.

### 2.2. Water analysis and Co speciation

Temperature, pH, conductivity, saturation and dissolved oxygen were measured using a multi-parameter field probe (Hach, IA, USA) just before biofilm sampling. Three samples (10 mL) of water were filtered through 0.45 µm cellulose acetate (CA) syringe filters (Ministart® NML, Startorius, Germany) and collected in polypropylene (PP) tubes (MetalFree®, Labcon, CA, USA) in each stream just before Co injection at each time point to determine dissolved metal concentrations. Three samples (10 mL) were additionally filtered on 0.45 µm CA filters and collected in PP tubes for cation and anion analyses with an additional two 50 mL samples filtered on 0.7 µm GF/F filters to be collected in burnt-amber glass flasks for dissolved organic carbon (DOC) concentrations at day 1, 7, 14, 21 and 28 in each stream. Cobalt concentrations in water were analyzed by Inductively Coupled Plasma Mass Spectrometry (ICP-MS model 7500, Agilent, CA, USA). The cation concentrations were measured by ICP-OES (Thermo iCAP 6000 Series, Thermo-

Fisher, MA, USA) and the anion concentrations were measured by ion chromatography (Dionex Aquion, Thermo-Fisher, MA, USA). SRLS-6 certified material (River water, CNRC, Canada) was used to calibrate the accuracy of the ICP-MS analyses (recovery of 103 ± 5 % for Co; n = 5) and the ICP-OES analyses (recovery of 98 ± 1 % for Ca<sup>2+</sup>; n = 3). The DOC concentrations were measured by a Shimadzu TOC-L analyzer (Japan). For modeling Co speciation, the Windermere Humic Aqueous Model (WHAM) model VII with its default data base was used (Bryan et al., 2002; Tipping, 2007). We assumed that 50 % of the dissolved organic matter (DOM) is made of carbon and that 65 % of the DOM is fulvic acid, the remainder was considered as inert.

### 2.3. Determination of Co bioaccumulation

For the analysis of intracellular Co concentrations, fresh biofilm samples were rinsed with 10 mM of ethylenediaminetetraacetic acid (EDTA, in disodium salt dihydrate form, Sigma-Aldrich, Germany) for 10 min to remove adsorbed metals on the surface of the biofilm whereas no rinsing step was performed for analyzing total Co concentrations (Meylan et al., 2003; Olguín and Sánchez-Galván, 2012). After that, samples were lyophilized and digested with 70 % HNO<sub>3</sub> and 30 % H<sub>2</sub>O<sub>2</sub> prior to mineralization (UltraWAVE™ oven, Milestone, Italy). Total and intracellular metal concentrations were analyzed by ICP-MS (ICP-MS model 7500, Agilent, CA, USA). BCR-414 certified reference material (plankton, JRC, Brussels) was used to confirm the sample digestion and the analytical accuracy (recovery of 83 ± 5 % for Co; n = 9). SLRS-6 was also used for this method to assess its accuracy (recovery of 108 ± 4 % for Co, n = 5).

### 2.4. Biofilm structure characterization

The quantity of dry biomass (in g<sub>dw</sub>) per glass slide area (cm<sup>2</sup>) was obtained from biofilm samples collected for Co bioaccumulation, chlorophyll *a* content, community structure and meta-metabolome analyses. Chlorophyll *a* contents were extracted with 10 mL of 90 % acetone (Uvasol®, Sigma-Aldrich, Germany), analyzed by spectrophotometry (Lambda 750, PerkinElmer, MA, USA) and quantified following the Jeffrey and Humphrey protocol (Jeffrey and Humphrey, 1975). Diatom analyses were carried out at the XPO platform (INRAE, Cestas, France; doi: 10.17180/brey-mr38) (INRAE institut, Cestas, France). Diatom cell density and mortality were determined from Lugol-preserved material for all replicate samples using a Nageotte counting chamber (Morin et al., 2010), under light microscopy (*Olympus BX51* upright microscope, 400× magnification). Diatom counts were reported as cells·cm<sup>-2</sup> of scraped substrate. The diatom replicate samples collected on day 28 were pooled to form one composite sample representative of the assemblage present for each Co condition. They were prepared according to the European standard EN ISO 13946 and counted using a Leica photomicroscope (oil immersion, 1000× magnification). A minimum of 400 individuals per sample (EN ISO 14407) were identified (Coste and Rosebery, 2011), with relative species abundance expressed as a %.

Subsequently to methanol extraction of metabolites, (described below in Section 2.5), DNA was extracted from the pellets of the same samples (Duperron et al., 2023) using the QIAGEN DNeasy® Power-Soil® Pro Kit DNA extraction kit following the manufacturer's instruction. The V4-V5 region of the 16S rRNA encoding gene was amplified using primers 515F (5'-GTGYCAGCMGCCGCGGTA-3') and 928R (5'-ACTYAAKGAATTGRCGGGG-3') (Wang and Qian, 2009). The V8-V9 region of the 18S rRNA encoding gene was amplified using primers V8F (5'-ATAACAGGTCTGTGATGCCCT-3') and 1510R (5'-CCTTCYGCAGGTTACCTAC-3') (Bradley et al., 2016). The amplicons were sequenced on an Illumina NextSeq 2000 300 × 2 bp platform (PGTB platform, Cestas, France; doi: 10.15454/1.5572396583599417E12). Sequence analyses were performed on the Galaxy FROGS pipeline (Afgan et al., 2018). Forward and reverse reads were timed at 280 and 275 bp, respectively. Amplicon Sequence Variants (ASVs) were obtained

with the default parameters and affiliated with the 16S SILVA 138.1 AND 18S SILVA 138.1 databases for prokaryote and eukaryote community characterization, respectively. Alpha- and beta-diversity metrics were computed in RStudio (v4.1.2) (R Core Team, 2021) with the R package phyloseq (v1.38.0) (McMurdie and Holmes, 2013) and pairwiseAdonis (v0.4) (Arbizu, 2022). Principal coordinates analyses (PCoA) based on weighted and unweighted UniFrac distances were performed to explore the prokaryotic and eukaryotic phylogenetic dissimilarity within groups (combination of exposure time and Co concentration). Inter-group and intra-group variance were computed with PERMANOVA (999 permutations) and PERMDISP (999 permutations), respectively.

## 2.5. Meta-metabolomic analyses

Untargeted meta-metabolomic analyses were performed at the PtSMB platform (Muséum National d'Histoire Naturelle, Paris, France) by LC-HRMS. From lyophilized biofilm samples (1 mg), metabolites were extracted with a solvent composed of 10  $\mu\text{L}$  cold 75 % methanol that was acidified with 0.1 % formic acid. Biofilm samples were then sonicated on ice (SONICS Vibra Cell, Newton, CT, USA; 130 W, 20 kHz; 80 % amplitude; 30 s) and centrifuged at 4 °C (12,000 g; 10 min) (Colas et al., 2020). Supernatants were harvested and stored in the dark at -20 °C.

For the mass spectrometry analysis, 2  $\mu\text{L}$  of the supernatants containing the metabolite extracts were analyzed by Ultra-high-performance liquid chromatography (UH-PLC) (ELUTE, Bruker, Bremen, Germany) using a Polar Advance II 2.5 pore C18 (Thermo Fisher Scientific, Waltham, MA, USA) chromatographic column (300  $\mu\text{L}\cdot\text{min}^{-1}$  over a linear gradient of acidified (0.1 % formic acid) acetonitrile from 5 to 90 % in 15 min) coupled with a high-resolution mass spectrometer (ESI-QqTOF, Compact, Bruker, Bremen, Germany) at 2 Hz frequency in positive MS mode in the range of 50–1500  $m/z$  (Le Moigne et al., 2021). The software MetaboScape 4.0 (Bruker, Bremen, Germany) was used to recalibrate the MS data. Ions with intensities above 5000 points in at least 10 % of all samples were selected. AutoMS/MS analysis was then conducted in positive mode for the qualitative study of metabolites. A molecular network was constructed with MetGem 1.3.6. and the comparison of fragmentation profiles and metabolite annotation was conducted.

### 2.5.1. Dose-response curve modeling and determination of the concentration range inducing defense and damage responses (CRIDeR/CRIDaR)

Untargeted meta-metabolomic features dose-response models were constructed using RStudio (v4.1.2) with the DRomics package (v2.5-0) (Larras et al., 2018). The biofilm meta-metabolomic response to  $\text{Co}^{2+}$  concentrations added in the exposure medium was determined at each time point. Half-minimum method for missing values was applied on the original data (peak intensity MS analysis) before  $\log_2$  transformation. Significantly responding untargeted meta-metabolomic features to Co concentrations were then selected using an ANOVA with a false discovery rate (FDR) of 0.05. Dose-response models with the best AICc (second-order Akaike's information criterion) were constructed. Benchmark-doses<sub>-1SD</sub> (BMD<sub>-1SD</sub>) were calculated from a benchmark-response<sub>-1SD</sub> (BMR<sub>-1SD</sub>); SD is the residual standard deviation of the considered model. The BMD<sub>-1SD</sub> represents the  $\text{Co}^{2+}$  concentration added in the exposure medium at which the response of each untargeted meta-metabolomic feature of exposed biofilms previously selected, differs from the response observed in control biofilms. Empirical cumulative density functions based on dose-response model trends (biphasic: bell- or U-shaped and monotonic: decreasing or increasing) were built in order to obtain an integrative response of biofilm untargeted meta-metabolomic features following Co exposure. On this basis, CRIDeR and CRIDaR initiation thresholds were determined for each time point from the best (with lowest AICc) fit model (e.g. Burr III, Gamma,

Gompertz, Inverse-Pareto, Gumbel, log-logistic, log-logistic/log-logistic mix, log-normal, log-normal/log-normal mix and Weibull distributions) for ECDFs of untargeted meta-metabolomic features with biphasic (bell- or U-shaped) and monotonic (decreasing or increasing) trends, respectively, with the R package ssdtools (v1.0.6) (Thorley and Schwarz, 2018). The CRIDeR and CRIDaR initiation thresholds are the hazardous concentrations at which 5 % of untargeted meta-metabolomic features with a biphasic or a monotonic trend, respectively, will potentially be affected on the basis of their BMDs<sub>-1SD</sub> (four additional hazardous threshold concentrations were also tested: 2, 10, 20 and 50 %). If all distributions failed to fit, the CRIDeR and CRIDaR initiation thresholds were determined directly with the BMD<sub>-1SD</sub> of the first untargeted meta-metabolomic feature impacted. The CRIDeRs end when the CRIDaRs begin.

### 2.5.2. Time-response curves modeling and determination of the time range inducing defense and damage responses (TRIDeR/TRIDaR)

Applying the same principle as CRIDeR/CRIDaR, untargeted meta-metabolomic features time-response models were built based on the biofilm meta-metabolomic response to Co exposure time for each exposure condition. After the  $\log_2$  transformation step, significantly responding untargeted meta-metabolomic features to Co exposure time were selected using an ANOVA with an FDR of 0.05. Dose-response models with the best AICc were also constructed. Benchmark-time<sub>-1SD</sub> (BMT<sub>-1SD</sub>) were calculated from a BMR<sub>-1SD</sub>. The BMT<sub>-1SD</sub> represents the exposure time (in days;  $\log_{10}$  transformed) at which the response of each untargeted meta-metabolomic feature of exposed biofilms previously selected differs from the response observed in control biofilms. Empirical cumulative density function construction and, TRIDeR and TRIDaR characterization were performed in the same way as for CRIDeR and CRIDaR (see Section 2.5.1). The TRIDeR and TRIDaR initiation thresholds are the hazardous exposure time at which 5 % of untargeted meta-metabolomic features with a biphasic or a monotonic trend, respectively, will potentially be affected on the basis of their BMTs<sub>-1SD</sub> (four additional hazardous exposure time were also tested: 2, 10, 20 and 50 %). If all distributions failed to fit, TRIDeR and TRIDaR initiation thresholds were determined directly with the BMT<sub>-1SD</sub> of the first untargeted meta-metabolomic feature impacted. The TRIDeRs end when the TRIDaRs begin.

## 2.6. Multivariate Omics Trajectory Analysis (MOTA)

The dynamics of biofilm meta-metabolome changes versus compositions of prokaryotic and eukaryotic biofilm communities were investigated by comparing trajectories of centroids using the Multivariate Omics Trajectory Analysis method (MOTA) (Foucault et al., 2022). Datasets of meta-metabolome, prokaryotic and eukaryotic biofilm communities were  $\log_2$  transformed and analyzed identically. Median distances between Principal Component Analyses' (PCA) centroid coordinates were computed by median to create a trajectory between each sampling time point for the four exposure conditions and displayed as the fraction of the total length achieved at each time point (from 0 to 100 % between hour 1 to day 28). Trajectories were plotted for the exposure time ( $\log_{10}$  transformed) versus meta-metabolomic data, 16S and 18S rRNA data for each exposure concentration, allowing comparison of their dynamics over time.

## 3. Results

### 3.1. Exposure conditions and media

The Gave de Pau water that flowed into the streams throughout the experiment had a pH of  $8.29 \pm 0.02$  (Table S1). Water temperature decreased during the exposure experiments, from  $13.67 \pm 0.31$  °C at the start of exposure (day 0) to  $10.28 \pm 0.04$  °C after 28 days (Table S1). The average background total dissolved Co concentration for 28 days was

$4.8 \pm 3.5 \times 10^{-9}$  M Co ( $1.36 \pm 0.85 \times 10^{-9}$  M  $\text{Co}^{2+}$ ),  $8.32 \pm 0.06 \times 10^{-4}$  M Ca,  $1.54 \pm 0.02 \times 10^{-4}$  M Mg,  $0.40 \pm 0.13$  mg DOC·L<sup>-1</sup> (Table S1). The averages of total dissolved Co concentrations for 28 days for each nominal condition ( $1 \times 10^{-7}$ ,  $5 \times 10^{-7}$  and  $1 \times 10^{-6}$  M) were  $0.92 \pm 0.07 \times 10^{-7}$ ,  $5.26 \pm 0.35 \times 10^{-7}$  and  $1.09 \pm 0.03 \times 10^{-6}$  M, respectively (Table S1). The corresponding average  $\text{Co}^{2+}$  concentrations were  $2.68 \pm 0.19 \times 10^{-8}$ ,  $1.68 \pm 0.16 \times 10^{-7}$  and  $3.06 \pm 0.34 \times 10^{-7}$  M, respectively.

### 3.2. Metal bioaccumulation

Mature biofilm naturally contained similar levels of total accumulated Co and intracellular Co, indicating that Co contents were almost entirely intracellular with an average intracellular Co of  $2.19 \pm 0.20 \times 10^{-7}$  mol·g<sub>DW</sub><sup>-1</sup>. This natural intracellular Co concentration remained constant throughout the experiment (Fig. 1 and Table S2). After 1 h, total and intracellular concentrations at all other time points significantly increased with exposure concentrations (*post-hoc* Dunn test,  $p < 0.05$ ; Figs. 1, S2 and Table S2). A bioaccumulation plateau was reached at day 14 for exposed biofilms (Fig. 1 and Table S2). At the end of exposure (day 28), the majority of accumulated Co by biofilms was intracellular ( $71 \pm 14$  %;  $n = 12$ ). Cobalt exposure concentrations had no effect on the biofilm bioaccumulation of other metals (Li, Al, Mn, Fe, Cu, Zn, As, Pb, Cd and Pb) present in the *Gave de Pau* (Table S3).

### 3.3. Biofilm structure

#### 3.3.1. Biomass and chlorophyll content

Biomass of control biofilms remained relatively stable over the 28-day experiment, with a slight but significant increase at days 3 and 7 (*post-hoc* Dunn test,  $p < 0.05$ , Table S3). In contrast, biofilm biomass was negatively impacted by Co exposure from day 14 (Fig. 2A, B and Table S4). On day 28, biofilm biomass decreased from  $142 \pm 12$  mg<sub>DW</sub>·cm<sup>-2</sup> in control biofilms to  $17.8 \pm 3.8$  mg<sub>DW</sub>·cm<sup>-2</sup> ( $-57$  %) and  $17.8 \pm 8.1$  ( $-58$  %) mg<sub>DW</sub>·cm<sup>-2</sup> at the two highest exposure concentrations ( $5 \times 10^{-7}$  and  $1 \times 10^{-6}$  M), respectively (*post-hoc* Dunn test,  $p <$

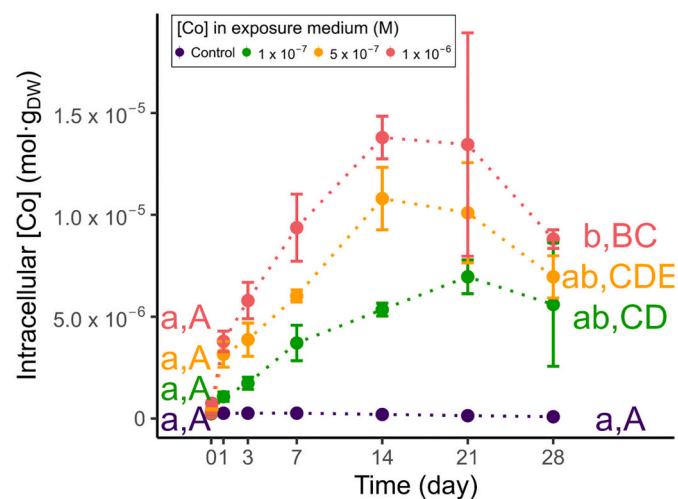


**Fig. 1.** Intracellular Co content (mol·g<sub>DW</sub><sup>-1</sup>) over time (day) according to Co concentration exposure groups (Control in blue,  $1 \times 10^{-7}$  M in green,  $5 \times 10^{-7}$  M in orange and  $1 \times 10^{-6}$  M in red). The lower-case letters correspond to the significant groups defined by a Dunn's *post-hoc* test ( $p < 0.05$ ) performed after Kruskal-Wallis non-parametric tests among Co exposure concentrations at each exposure time. Capital letters correspond to the significant groups defined by a Dunn's *post-hoc* test ( $p < 0.05$ ) performed after Kruskal-Wallis non-parametric tests among the exposure times for each exposure concentration. To improve make the graph easier to readability, only test results for days 0 and day 28 are displayed. Significance of tests at intermediate time points are displayed in Table S2.

0.05). No effect was observed at  $1 \times 10^{-7}$  M Co at any exposure time.

Chlorophyll *a* content increased by a factor of 4- and 2.4-fold during the 28-day experiment in control biofilms and biofilms exposed to  $1 \times 10^{-7}$  M Co, respectively. At  $5 \times 10^{-7}$  and  $1 \times 10^{-6}$  M Co, chlorophyll *a* content decreased from  $5.3 \pm 1.1$  in control biofilms to  $2.10 \pm 0.72$  ( $-61$  %) and  $1.8 \pm 1.3$  ( $-65$  %)  $\mu\text{g}_{\text{DW}}\cdot\text{cm}^{-2}$ , respectively (*post-hoc* Dunn test,  $p < 0.05$ ; Fig. 2B and Table S4). On day 28, the BMD<sub>-1SD</sub> calculated for chlorophyll *a* content was  $3.73 \times 10^{-8}$  M.

#### 3.3.2. Prokaryotic biofilm community analysis

Analysis of prokaryotic community compositions based on the V4-V5 region of the 16S rRNA-encoding gene from the 192 biofilm metabolite-extract samples yielded 13,903,832 raw reads. Of which, 90.6 % were retained after sequence assembly, denoising and chimera removal, and 74.1 % were retained after a clustering filter (cluster with at least 0.005 % of all sequences). Samples displayed from 41,886 to 121,693 reads (mean  $69,951 \pm 13,765$  reads). Finally, 2012 prokaryotic ASVs were taxonomically assigned.

At the first sampling time (1 h), the ASVs richness of control biofilms was  $1866 \pm 15$  ASVs (Fig. S3A). It remained constant up to 21 d of exposure, whereby it later significantly decreased by 13.3 %; with comparable richness values found at days 21 and 28. Similar effects of exposure time were observed in Co-exposed biofilms. The ASVs richness decrease was exacerbated by Co at 28 d of exposure. It significantly decreased by 28.1 %, 27.0 % and 32.3 % when compared to control biofilms at  $1 \times 10^{-7}$  M,  $5 \times 10^{-7}$  M and  $1 \times 10^{-6}$  M, respectively (*post-hoc* Dunn test,  $p < 0.05$ ). The decreased ASVs richness of control biofilms at days 21 and 28 were accompanied by a significant 10 % decrease in evenness (Fig. S3B). In biofilms exposed to  $1 \times 10^{-7}$  M and  $5 \times 10^{-7}$  M Co, a significant decrease in evenness was observed at day 14, whereas it was only significant for biofilms exposed to the highest Co concentration at days 21 and 28. This decreased evenness was higher in biofilms exposed to  $1 \times 10^{-6}$  M Co for 28 d, with a value of  $0.67 \pm 0.02$  as compared to the value of  $0.75 \pm 0.02$  observed for control biofilms (*post-hoc* Dunn test,  $p < 0.05$ ). The Shannon index also significantly decreased in control biofilms after 21 and 28 d of exposure (Fig. S3C); a significant decrease from 6.34 to 5.66 and 5.56 were measured at days 21 and 28, respectively. With the Co exposures, a larger significant decrease was observed, with Shannon index decreases to 5.03, 4.93 and 4.76 in biofilms exposed to  $1 \times 10^{-7}$  M,  $5 \times 10^{-7}$  M and  $1 \times 10^{-6}$  M, respectively, on day 28 (*post-hoc* Dunn test,  $p < 0.05$ ).

Control prokaryotic communities analyzed after 1 h of exposure consisted of over 16 identified classes, with a predominance of Cyanobacteria ( $27.9 \pm 0.1$  %), Bacteroidia ( $14.8 \pm 0.0$  %), Planctomycetes ( $13.3 \pm 0.0$  %), Gammaproteobacteria ( $12.5 \pm 0.0$  %) and Alphaproteobacteria ( $7.5 \pm 0.0$  %) (Fig. S4A). Visually, samples from different time points were well dispersed along the first axis of the PCoA, and exposure concentrations were rather separated on the second axis of the PCoA (Fig. 3A and B). At that early exposure time (1 h), the compositions of prokaryotic communities exposed to  $5 \times 10^{-7}$  and  $1 \times 10^{-6}$  M Co were already significantly different from those of the control biofilms (Unweighted UniFrac; PERMANOVA,  $p < 0.05$ ; Fig. 3A and Table S5). A significant decrease in the relative abundance of vadinHA49 (Planctomycetota) (*post-hoc* Dunn test,  $p < 0.05$ ) and an increase in the relative abundance of Alphaproteobacteria (*post-hoc* Dunn test,  $p < 0.05$ ) in biofilms exposed to  $1 \times 10^{-6}$  M were observed compared to those in control biofilms (Fig. S4A). After 1 d of exposure, prokaryotic community compositions were significantly different only between those of control biofilms and those exposed to  $5 \times 10^{-7}$  M (Unweighted UniFrac; PERMANOVA,  $p < 0.05$ ; Fig. 3A and Table S5). On day 3, no significant differences were observed. On day 7, prokaryotic community compositions and diversities were significantly different only between control biofilms and biofilms exposed to  $1 \times 10^{-6}$  M (Unweighted UniFrac and Weighted UniFrac; PERMANOVA,  $p < 0.05$ ; Fig. 3A, B and Table S5). From day 14 to the end of the experiment (day 28), prokaryotic community compositions differed significantly between biofilms from the

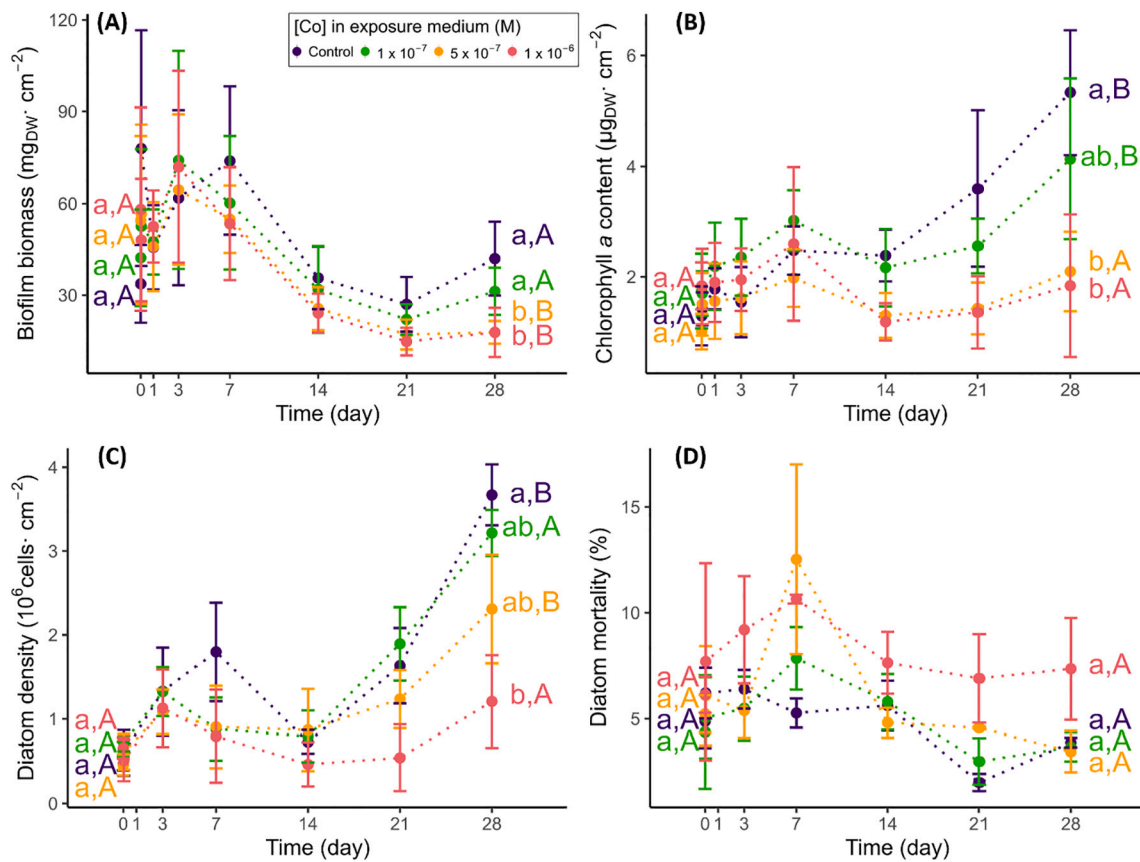


**Fig. 2.** Effects of Co on traditional biological parameters of river biofilms (Control in blue, 1 × 10<sup>-7</sup> M in green, 5 × 10<sup>-7</sup> M in orange and 1 × 10<sup>-6</sup> M in red). (A) Biofilm biomass (mg<sub>DW</sub>·cm<sup>-2</sup>) as a function of time (day) according to Co exposure concentrations. (B) Biofilm chlorophyll a content (µg<sub>DW</sub>·cm<sup>-2</sup>) as a function of time (day) according to Co exposure concentrations. (C) Diatom density (10<sup>6</sup> cells·cm<sup>-2</sup>) as a function of time (day) according to Co exposure concentrations. (D) Diatom mortality (% of death cells) as a function of time (day) according to Co exposure concentrations. The lower-case letters correspond to the significant groups defined by a Dunn's *post-hoc* test (*p* < 0.05) performed after Kruskal-Wallis non-parametric tests among Co exposure concentrations at each exposure time. Capital letters correspond to the significant groups defined by a Dunn's *post-hoc* test (*p* < 0.05) performed after Kruskal-Wallis non-parametric tests among the exposure times for each exposure concentration. Only test results for days 0 and 28 are displayed, to make the graph easier to read. Significance of tests at intermediate time points are displayed in Table S4.

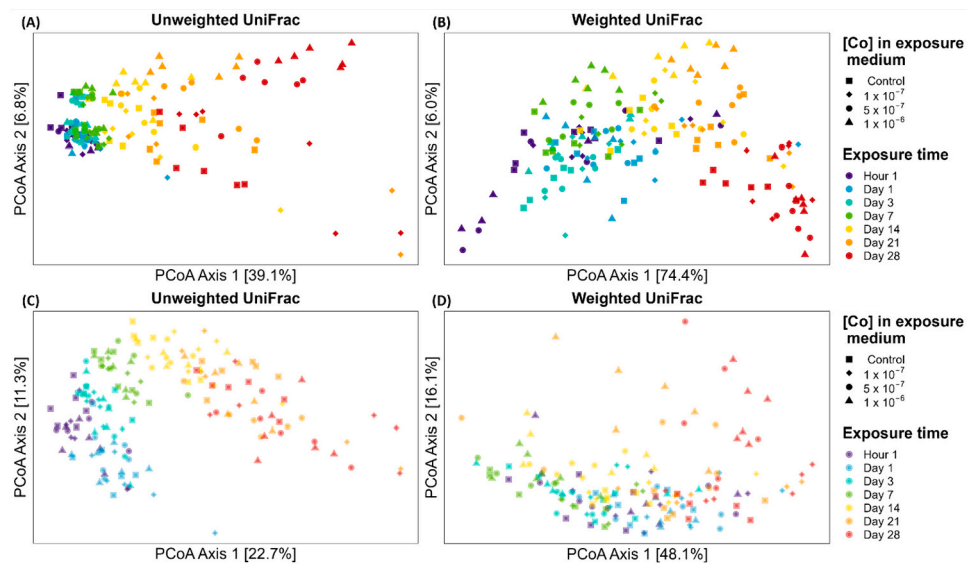


**Fig. 3.** Effects of cobalt concentrations and exposure time on biofilm composition and diversity. (A) PCoA on prokaryotic community (Unweighted UniFrac distance). (B) PCoA on prokaryotic community (Weighted UniFrac distance). (C) PCoA on eukaryotic community (Unweighted UniFrac distance). (D) PCoA on eukaryotic community (Weighted UniFrac distance).

control group and biofilms exposed to  $5 \times 10^{-7}$  and  $1 \times 10^{-6}$  M (Unweighted UniFrac; PERMANOVA,  $p < 0.05$ ; Fig. 3A and Table S5). At days 21 and 28, prokaryotic community diversities differed significantly between biofilms from the control group and biofilms exposed to  $5 \times 10^{-7}$  and  $1 \times 10^{-6}$  M (Weighted UniFrac; PERMANOVA,  $p < 0.05$ ; Fig. 3B and Table S5). Prokaryotic community diversities were also significantly different in biofilms exposed to  $1 \times 10^{-7}$  and  $1 \times 10^{-6}$  M, and in biofilms exposed to  $5 \times 10^{-7}$  and  $1 \times 10^{-6}$  M (Weighted UniFrac; PERMANOVA,  $p < 0.05$ ; Fig. 3B and Table S5). At day 28, an increase in the relative abundance of the dominant Cyanobacteria class as a function of Co concentrations was observed, as well as a decrease of Polyangia, vadinHA49, KD4–96 (Chloroflexi) and OM190 (Planctomycetota) (*post-hoc* Dunn test,  $p < 0.05$ ; Fig. S4A). The diversities of prokaryotic communities of biofilms exposed to  $1 \times 10^{-7}$  M were never different from those of biofilms exposed to  $5 \times 10^{-7}$  M throughout the experiment whereas they were significantly different from those of biofilms exposed to  $1 \times 10^{-6}$  M on days 14 and 28 (Unweighted UniFrac; PERMANOVA,  $p < 0.05$ ; Fig. 3A and Table S5). The diversities of prokaryotic communities of biofilms exposed to the two highest Co concentrations ( $5 \times 10^{-7}$  and  $1 \times 10^{-6}$  M) were significantly different only after 28 d (Unweighted UniFrac; PERMANOVA,  $p < 0.05$ ; Fig. 3A and Table S5). Taking temporal dynamics into account, the prokaryotic community composition of biofilms in the control group were different between 1 h and 7, 14, 21 and 28 d (Unweighted UniFrac; PERMANOVA,  $p < 0.05$ ; Fig. 3A and Table S5). Prokaryotic community composition for biofilms exposed to Co were different between hour 1 and day 1, yet were similar between hour 1 and day 3. As the experiment continued, compositions on day 3 differed from those on day 7, whereby the composition did not change significantly for the remainder of experimentation (day 28) (Unweighted UniFrac; PERMANOVA,  $p < 0.05$ ; Fig. 3A and Table S5). It is important to note that the diversity of all prokaryotic communities differed significantly from those of the control biofilms after 14 d of exposure (Weighted UniFrac; PERMANOVA,  $p < 0.05$ ; Fig. 3B and Table S5).

### 3.3.3. Eukaryotic biofilm community analysis

Analysis of eukaryotic community composition within the V8-V9 region of the 18S rRNA-encoding gene of the 192 biofilm metabolite-extract samples yielded 46,994,861 raw reads, of which 73.4 % were retained after sequence assembly, denoising and chimera removal, and 67.8 % were retained after a clustering filter (cluster with at least 0.005 % of all sequences). Samples displayed 76,931 to 398,084 reads ( $230,159 \pm 49,366$ ). Finally, 902 eukaryotic ASVs were taxonomically assigned.

At the first sampling time (1-h exposure), the richness of control biofilms was  $745 \pm 15$  ASVs (Fig. S5A) and remained constant throughout the remainder of the experiment. At day 28, Co exposure induced a significant decrease by 14.9 %, 10.7 % and 17.1 % in biofilms exposed to  $1 \times 10^{-7}$  M,  $5 \times 10^{-7}$  M and  $1 \times 10^{-6}$  M, respectively (*post-hoc* Dunn test,  $p < 0.05$ ). The evenness was also similar in control biofilms over time, with a median value of 0.57 (Fig. S5B). In biofilms exposed to  $5 \times 10^{-7}$  M and  $1 \times 10^{-6}$  M Co, a significant increase in evenness was observed by as early as day 14. At day 28, Co concentration induced a 15.2 % and 17.1 % significant increase in evenness, respectively (*post-hoc* Dunn test,  $p < 0.05$ ). The Shannon index was also similar in control biofilms over time, with a median value of 3.80 (Fig. S5C). In biofilms exposed to  $5 \times 10^{-7}$  M and  $1 \times 10^{-6}$  M Co, a significant increase in the Shannon index was observed by day 14, and by day 28, Co concentration induced a significant increase to 4.24 and 4.31, respectively (*post-hoc* Dunn test,  $p < 0.05$ ).

Bacillariophyceae (diatoms) represented >50 % of the relative abundances in all samples (Fig. S4B). The remaining classes were mostly Clitellata (11 %) and Catenulida (11 %). Visually, samples from different time points were well dispersed along the first axis of the PCoA, and exposure concentrations were rather separated on the second axis of the PCoA (Fig. 3C and D). After 1 h of exposure, the composition and the

diversity of eukaryotic communities were not impacted by Co exposure. From day 14 to the end of the experiment, eukaryotic community compositions were significantly different between those of control biofilms and those of biofilms exposed to the two highest concentrations ( $5 \times 10^{-7}$  and  $1 \times 10^{-6}$  M), while those of biofilms exposed to  $1 \times 10^{-7}$  M were only different from the control group on day 14 (Unweighted UniFrac; PERMANOVA,  $p < 0.05$ ; Fig. 3C and Table S6). From day 14 to day 28, eukaryotic community diversity was significantly different between the control biofilm and the biofilm exposed to the highest concentration (Weighted UniFrac; PERMANOVA,  $p < 0.05$ ; Fig. 3D and Table S6). At days 14 and 28, eukaryotic community diversities were also significantly different in control biofilm and in biofilm exposed to  $5 \times 10^{-7}$  M (Weighted UniFrac; PERMANOVA,  $p < 0.05$ ; Fig. 3D and Table S6). On days 14, 21 and 28, all eukaryotic community compositions were significantly different between each group of exposed biofilms (except between  $1 \times 10^{-7}$  and  $5 \times 10^{-7}$  M on day 28) (Unweighted UniFrac; PERMANOVA,  $p < 0.05$ ; Fig. 3C and Table S6). By day 28, an increase as a function of Co concentrations of relative abundance of Chlorophyceae, Eustigmatophyceae and Ulvophyceae was observed as well as a decrease of Bacillariophyceae and Catenulida (*post-hoc* Dunn test,  $p < 0.05$ ; Fig. S4B). Taking temporal dynamics into account, all eukaryotic community compositions differed significantly from those of the control biofilms after 1 d of exposure (except for those of biofilms exposed to  $5 \times 10^{-7}$  and  $1 \times 10^{-6}$  M on day 3) (Unweighted UniFrac; PERMANOVA,  $p < 0.05$ ; Fig. 3C and Table S6). The diversity of all eukaryotic communities differed significantly from those of the control biofilms after 7 d of exposure (except for those of biofilms exposed to  $5 \times 10^{-7}$  and  $1 \times 10^{-6}$  M on day 7) (Weighted UniFrac; PERMANOVA,  $p < 0.05$ ; Fig. 3D and Table S6).

### 3.3.4. Diatom composition and mortality

Microscopy observations were in agreement with genomic analyses and revealed that diatoms dominated the autotrophic community. Diatom densities significantly decreased only at day 28, from  $3.67 \pm 0.36$  to  $2.31 \pm 0.65$  (−37 %) and  $1.21 \pm 0.55$  (−67 %)  $\times 10^6$  cells·cm<sup>−2</sup> at the two highest exposure concentrations, respectively (Fig. 2C, Table S4) (*post-hoc* Dunn test,  $p < 0.05$ ). A significant increase in diatom mortality was observed on day 21 in biofilms exposed to  $1 \times 10^{-6}$  M, rising from  $2.02 \pm 0.04$  in the control group to  $6.90 \pm 0.21$  % (+242 %) (Fig. 2D and Table S4) (*post-hoc* Dunn test,  $p < 0.05$ ). Although not significant, the higher Co concentration induced greater diatom mortality at each time point than that observed in the control group. The lowest concentration ( $1 \times 10^{-7}$  M) had no significant effect on these biological parameters (Fig. 2C, D and Table S4). Cobalt exposure led to changes in diatom community composition, with a decrease in *Achnanthis* F.T. Kützing spp. and *Cocconeis placentula* Ehrenberg var. *lineata* (Ehr.) Van Heurck and an increase in *Eolimna minima* (Grunow) Lange-Bertalot, *Fragilaria capucina* Desmazières var. *capucina*, *Fragilaria capucina* Desmazières var. *vaucheriae* (Kützing) Lange-Bertalot, *Fragilaria crotonensis* Kitton, *Gomphonema parvulum* (Kützing) Kützing var. *parvulum* f. *parvulum* and *Mayamaea atomus* var. *permissis* Hustedt Lange-Bertalot (Fig. S6 and Table S7).

## 3.4. Biofilm meta-metabolomic fingerprints

### 3.4.1. Untargeted meta-metabolomic features

In total, 5141 untargeted meta-metabolomic features were observed among all samples while only 192 (3.7 %) annotations were attempted using the molecular network approach supported by public spectral database inquiry. However, over 92 % of the global meta-metabolome appeared significantly impacted during the 28 d of exposure. Cobalt concentrations had a significant effect on the contents of 2356 untargeted meta-metabolomic features, exposure time on the contents of 4703 untargeted meta-metabolomic features and their interaction induced a change in the contents of 1950 untargeted meta-metabolomic features (two-way ANOVA,  $p < 0.05$ ).

A gradual change over time in the meta-metabolomic fingerprints of biofilms with the influence of Co exposure concentrations was observed (Fig. S7A). Except at day 7, the meta-metabolomic fingerprints of control biofilms at each time point studied were different from those at the first-time point (hour 1) (PERMANOVA,  $p < 0.05$ ; Table S8). After 1 h of exposure, the meta-metabolomic fingerprints were already different between the control and Co-exposed biofilms (PERMANOVA,  $p < 0.05$ ; Table S8). On days 1, 3, 7 and 14, the meta-metabolic fingerprints of biofilms showed no significant differences between control and exposed biofilms (PERMANOVA; Table S8). At day 21, the meta-metabolomic

fingerprints were significantly different when comparing control biofilms and biofilms exposed to  $5 \times 10^{-7}$  and  $1 \times 10^{-6}$  M Co (PERMANOVA,  $p < 0.5$ ; Table S8). After 28 d of exposure, the meta-metabolomic fingerprints of the control biofilms and biofilms exposed to  $1 \times 10^{-7}$  M were significantly different from those of the biofilms exposed to the two highest Co concentrations ( $5 \times 10^{-7}$  and  $1 \times 10^{-6}$  M) (PERMANOVA,  $p < 0.05$ ; Table S8). Moreover, the meta-metabolomic fingerprints of biofilms exposed to  $5 \times 10^{-7}$  M were also significantly different from those of biofilms exposed to  $1 \times 10^{-6}$  M (PERMANOVA,  $p < 0.05$ ; Table S8).

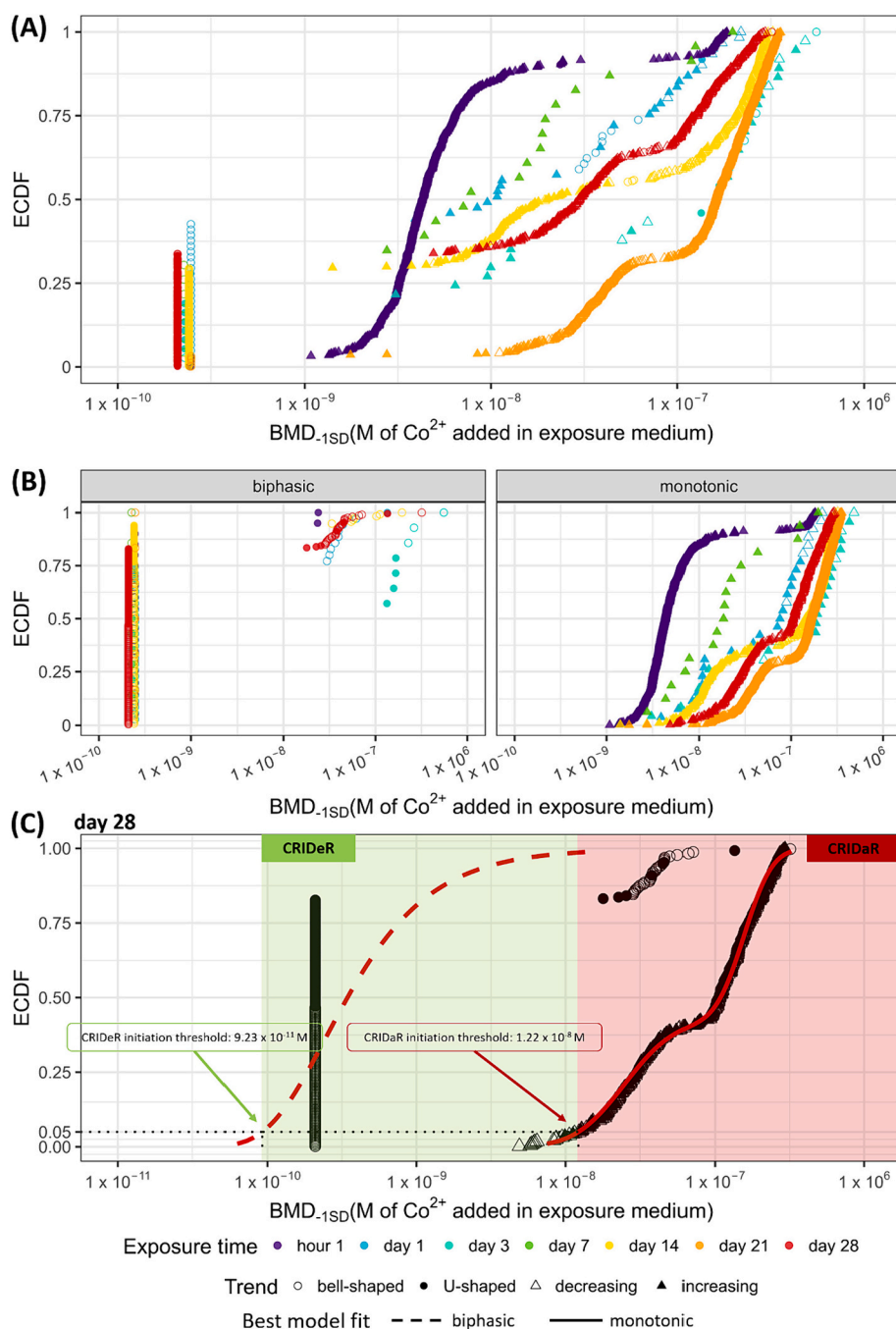


**Fig. 4.** Biofilm meta-metabolomic responses to Co concentrations. (A) Distribution of  $BMD_{-1SD}$  (M of  $Co^{2+}$  added in exposure medium) as an ECDF at each sampling time step. (B) Distribution of  $BMD_{-1SD}$  (M of  $Co^{2+}$  added in exposure medium) as an ECDF split by trend of dose-response curve; biphasic (bell- and U-shaped) or monotonic (decreasing and increasing). (C) Determination of CRIDeR and CRIDaR initiation thresholds at day 28 from the best fit model for ECDFs of untargeted meta-metabolomic features with biphasic (bell- or U-shaped) and monotonic (decreasing or increasing) trends, respectively. CRIDeR and CRIDaR initiation thresholds are the hazardous concentration at which 5% of untargeted meta-metabolomic features will potentially be affected on the basis of their  $BMDs_{-1SD}$ . Determination of CRIDeR and CRIDaR initiation thresholds for the other sampling time is presented in Fig. S9 and Table 1.

3.4.2. Annotated metabolites in biofilms

Over 97 % of the 192 annotated metabolites were significantly impacted during the 28 days of exposure. Cobalt concentrations had a significant effect on the levels of 143 metabolites, while exposure time on the levels of 186 metabolites and their interaction induced a change in the levels of 123 metabolites (two-way ANOVA,  $p < 0.05$ ).

Various families of metabolites were observed, such as flavonoids, amino acids, nucleic acids and many lipids or lipid precursors, including lyso-diacylglyceryltrimethylhomoserines (LDGTS), lysophosphatidylcholines (LPC), phosphatidylethanolamines (PE) and steroids (Fig. S8 and Table S9). Globally, considering the entire meta-metabolome, similar trends were observed for the 3.7 % of untargeted meta-metabolomic features that have been annotated (Table S9). The application of similar data processing better evidenced the influence of Co concentration and exposure time using the whole meta-metabolome data set than the 192 annotated metabolites (Fig. S7B).

3.4.3. Dose-response curve trends of untargeted meta-metabolomic features as a sensitive indicator of biofilm responses to Co concentrations

Dose-response models were built based on the peak intensity of the untargeted meta-metabolomic features as a function of added Co concentrations in exposure media for each time point. They were then classified into four different categories as a function of their respective curve trends. In total, the dose-response curves of 285 features exhibited a bell-shaped trend, 118 a U-shaped trend, 1051 an increasing trend and 783 a decreasing trend (Fig. 4A and Table S10). Using ECDF curves to aggregate (Fig. 4B) the BMDs<sub>-1SD</sub> retrieved from those dose-response curves, CRIDeR initiation thresholds were determined from the best fit model at each time point (Table S11). These thresholds correspond to the hazardous concentrations at which 5 % of untargeted meta-metabolomic features with a biphasic dose-response trend will potentially be affected on the basis of their BMDs<sub>-1SD</sub> (Figs. 4C and S9). Note that 2, 10, 20 and 50 % were also tested, and the effect on the CRIDeR/CRIDaR threshold initiation values are described in Text S1. The Co

**Table 1**

Calculated CRIDeR and CRIDaR at each time point. \* CRIDeR threshold determined directly with the BMD<sub>-1SD</sub> of the first untargeted meta-metabolomic feature impacted because all distributions failed to fit.

| Time point | Concentration range | CRIDeR<br>(M of Co <sup>2+</sup> added in exposure medium) |       | CRIDaR<br>(M of Co <sup>2+</sup> added in exposure medium) |       | Pearson's $\chi^2$ test                           |      |                          |
|------------|---------------------|--|-------|--|-------|---|------|--------------------------|
|            | Trend               | Number   | %     | Number   | %     | $\chi^2$  | d.f. | p-Value                  |
| Hour 1     | Concentration range | 1.55 × 10 <sup>-10</sup> – 1.93 × 10 <sup>-9</sup>         |       | 1.93 × 10 <sup>-9</sup> –                                  |       | With simulated p-value (based on 2000 replicates) |      |                          |
|            | Bell-shaped         | 18   | 100.0 | 0  | 0.0   |   |      |                          |
|            | U-shaped            | 0  | 0.0   | 2  | 100.0 |   |      |                          |
|            | Increasing          | 17   | 3.1   | 535  | 96.9  |   |      |                          |
|            | Decreasing          | 0  | 0.0   | 0  | 0.0   |   |      |                          |
|            | Biphasic            | 18   | 90.0  | 2  | 10.0  | 253.8429  | NA   | 5.00 × 10 <sup>-4</sup>  |
| Day 1      | Monotonic           | 17   | 3.1   | 535  | 96.9  | With Yates' continuity correction                 |      |                          |
|            | Concentration range | 8.65 × 10 <sup>-11</sup> – 5.26 × 10 <sup>-9</sup>         |       | 5.26 × 10 <sup>-9</sup> –                                  |       |   |      |                          |
|            | Bell-shaped         | 23   | 74.2  | 8  | 25.8  |   |      |                          |
|            | U-shaped            | 3  | 75.0  | 1  | 25.0  |   |      |                          |
|            | Increasing          | 1  | 5.3   | 18   | 94.7  |   |      |                          |
|            | Decreasing          | 0  | 0.0   | 7  | 100.0 | 27.21555  | 1    | 1.82 × 10 <sup>-7</sup>  |
| Day 3      | Biphasic            | 26   | 74.3  | 9  | 25.7  | With simulated p-value (based on 2000 replicates) |      |                          |
|            | Monotonic           | 1  | 3.8   | 25   | 96.2  |   |      |                          |
|            | Concentration range | 1.14 × 10 <sup>-11</sup> – 4.11 × 10 <sup>-9</sup>         |       | 4.11 × 10 <sup>-9</sup> –                                  |       |   |      |                          |
|            | Bell-shaped         | 1  | 25.0  | 3  | 75.0  |   |      |                          |
|            | U-shaped            | 6  | 60.0  | 4  | 40.0  |   |      |                          |
|            | Increasing          | 1  | 5.6   | 17   | 94.4  |   |      |                          |
| Day 7      | Decreasing          | 0  | 0.0   | 5  | 100.0 |   |      |                          |
|            | Biphasic            | 7  | 50.0  | 7  | 50.0  | 10.70268  | NA   | 1.00 × 10 <sup>-3</sup>  |
|            | Monotonic           | 1  | 4.3   | 22   | 95.7  | With simulated p-value (based on 2000 replicates) |      |                          |
|            | Concentration range | 2.26 × 10 <sup>-10</sup> – 2.88 × 10 <sup>-9</sup>         |       | 2.88 × 10 <sup>-9</sup> –                                  |       |   |      |                          |
|            | Bell-shaped         | 7  | 100.0 | 0  | 0.0   |   |      |                          |
|            | U-shaped            | 0  | 0.0   | 0  | 0.0   |   |      |                          |
| Day 14     | Increasing          | 1  | 6.3   | 15   | 93.8  |   |      |                          |
|            | Decreasing          | 0  | 0.0   | 0  | 0.0   |   |      |                          |
|            | Biphasic            | 7  | 100.0 | 0  | 0.0   | 18.86719  | NA   | 5.00 × 10 <sup>-4</sup>  |
|            | Monotonic           | 1  | 6.3   | 15   | 93.8  | With Yates' continuity correction                 |      |                          |
|            | Concentration range | 1.69 × 10 <sup>-10</sup> – 6.40 × 10 <sup>-9</sup>         |       | 6.40 × 10 <sup>-9</sup> –                                  |       |   |      |                          |
|            | Bell-shaped         | 88   | 92.6  | 7  | 7.4   |   |      |                          |
| Day 21     | U-shaped            | 21   | 100.0 | 0  | 0.0   |   |      |                          |
|            | Increasing          | 8  | 8.1   | 91   | 91.9  |   |      |                          |
|            | Decreasing          | 1  | 0.6   | 155  | 99.4  |   |      |                          |
|            | Biphasic            | 109  | 94.0  | 7  | 6.0   | 292.5925  | 1    | 1.35 × 10 <sup>-65</sup> |
|            | Monotonic           | 10   | 3.5   | 245  | 96.5  | With simulated p-value (based on 2000 replicates) |      |                          |
|            | Concentration range | 2.48 × 10 <sup>-10</sup> – 2.00 × 10 <sup>-8</sup>         |       | 2.00 × 10 <sup>-8</sup> –                                  |       |   |      |                          |
| Day 28     | Bell-shaped         | 6  | 100.0 | 0  | 0.0   |   |      |                          |
|            | U-shaped            | 0  | 0.0   | 0  | 0.0   |   |      |                          |
|            | Increasing          | 15   | 7.3   | 178  | 92.7  |   |      |                          |
|            | Decreasing          | 15   | 3.2   | 455  | 96.8  |   |      |                          |
|            | Biphasic            | 6  | 100.0 | 0  | 0.0   | 106.4548  | NA   | 5.00 × 10 <sup>-4</sup>  |
|            | Monotonic           | 31   | 4.4   | 632  | 95.6  | With Yates' continuity correction                 |      |                          |
| Day 28     | Concentration range | 9.23 × 10 <sup>-11</sup> – 1.22 × 10 <sup>-8</sup>         |       | 1.22 × 10 <sup>-8</sup> –                                  |       |   |      |                          |
|            | Bell-shaped         | 96   | 77.4  | 28   | 22.6  |   |      |                          |
|            | U-shaped            | 74   | 91.4  | 7  | 8.6   |   |      |                          |
|            | Increasing          | 12   | 7.8   | 142  | 92.2  |   |      |                          |
|            | Decreasing          | 2  | 1.4   | 143  | 98.6  |   |      |                          |
|            | Biphasic            | 170  | 82.9  | 35   | 17.1  | 317.8485  | 1    | 4.26 × 10 <sup>-71</sup> |
| Monotonic  | 14                  | 4.7  | 285   | 95.3   |       |   |      |                          |

concentrations initiating CRiDeRs were found to be comparable at each exposure time:  $1.55 \times 10^{-10}$ ,  $8.65 \times 10^{-11}$ ,  $1.14 \times 10^{-11}$ ,  $2.26 \times 10^{-10}$ ,  $1.69 \times 10^{-10}$ ,  $2.48 \times 10^{-10}$  and  $9.23 \times 10^{-11}$  M of  $\text{Co}^{2+}$  added in exposure medium, respectively (Figs. 4, S9 and Table 1). The CRiDaR

initiation thresholds were also determined from the best fit model at each time point (Table S11) and correspond to the hazardous concentrations at which 5 % of untargeted meta-metabolomic features with a monotonic dose-response trend will potentially be affected on the basis

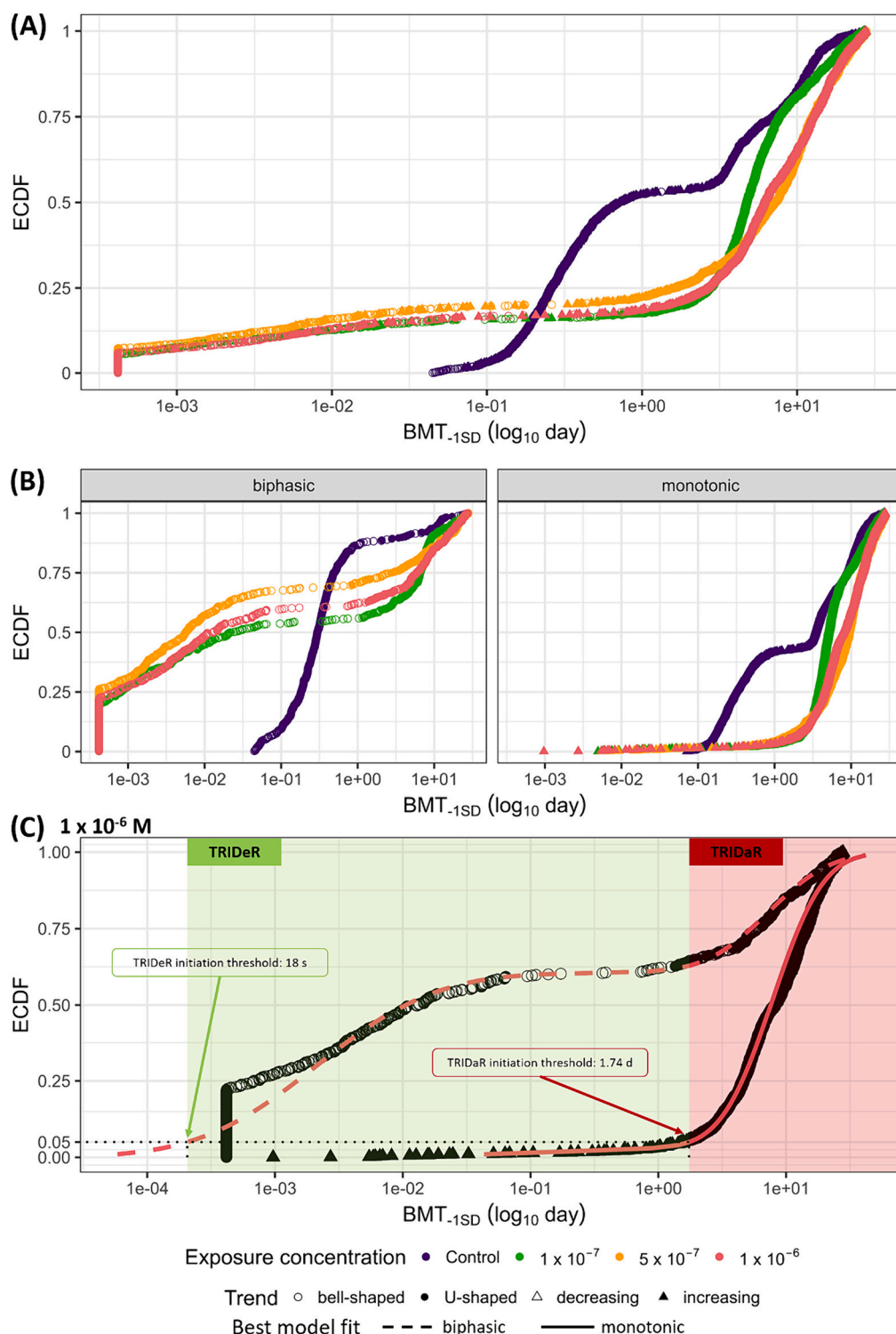


**Fig. 5.** Biofilm meta-metabolomic responses to Co exposure times. (A) Distribution of  $\text{BMT}_{-1\text{SD}}$  (in days;  $\log_{10}$  transformed) as an ECDF for each exposure concentration. (B) Distribution of  $\text{BMT}_{-1\text{SD}}$  (in days;  $\log_{10}$  transformed) as an ECDF split by trend of dose-response curve; biphasic (bell- and U-shaped) or monotonic (decreasing and increasing). (C) Determination of TRiDeR and TRiDaR initiation thresholds for  $1 \times 10^{-5}$  M exposure concentration from the best fit model for ECDFs of untargeted meta-metabolomic features with biphasic (bell- or U-shaped) and monotonic (decreasing or increasing) trends, respectively. TRiDeR and TRiDaR initiation thresholds are the hazardous exposure time at which 5 % of untargeted meta-metabolomic features will potentially be affected on the basis of their  $\text{BMTs}_{-1\text{SD}}$ . Determination of TRiDeR and TRiDaR initiation thresholds for the other sampling times are presented in Fig. S10 and Table 2.

of their BMDs<sub>-1SD</sub> (Figs. 4C and S9). The Co concentrations initiating CRIDaRs increased gradually over time; starting at  $1.93 \times 10^{-9}$  by hour 1, increasing to  $4. \times 10^{-9}$  by day 3 and  $6.40 \times 10^{-9}$  by day 14, ending at  $2.00 \times 10^{-8}$  and  $1.22 \times 10^{-8}$  M by days 21 and 28, respectively (Figs. 4, S9 and Table 1).

After 1 h of exposure, 90 % of untargeted meta-metabolomic features with biphasic dose-response trends were present in the CRIDeR (Table 1). That percentage decreased to 74.3 % and 50.0 % at days 1 and 3 (Table 1). By day 7, 100 % of the untargeted meta-metabolomic features with biphasic dose-response trends were present in CRIDeR, whereas 94.0 %, 100 % and 82.9 % were present at 14, 21 and 28 d, respectively (Table 1). At each time point, 96.9 %, 96.2 %, 95.7 %, 93.8 %, 96.1 %, 95.3 % and 95.3 %, respectively, of untargeted meta-metabolomic features with monotonic trends were present in CRIDaR (Table 1). The proportions of untargeted meta-metabolomic features with biphasic dose-response trends (bell-shaped and U-shaped) were significantly greater in CRIDeR than in CRIDaR (Pearson's  $\chi^2$  test,  $p < 0.001$ ; Table 1). Conversely, the proportions of untargeted meta-metabolomic features with monotonic dose-response trends (increasing and decreasing) were significantly greater in CRIDaR than in CRIDeR (Pearson's  $\chi^2$  test,  $p < 0.001$ ; Table 1).

#### 3.4.4. Time-response curve trends of untargeted meta-metabolomic features as a sensitive indicator of biofilm responses to Co exposure

Time-dose models were constructed based on the intensity of the metabolomic feature peaks as a function of time for each exposure with Co<sup>2+</sup> added to the exposure medium. The curves were further classified into four different categories as a function of their respective time-response model curve trend. In total, 1784 exhibited a bell-shaped trend, 235 a U-shaped trend, 5443 an increasing trend and 177 a decreasing trend (Fig. 5 and Table S12). Using ECDF curves to aggregate (Fig. 5B) the BMTs<sub>-1SD</sub> retrieved for those dose-response curves, TRIDeR initiation exposure times were determined from the best fit model at each time point (Table S13), and correspond to the hazardous times where 5 % of untargeted meta-metabolomic features with a biphasic dose-response trend will potentially be affected on the basis of their BMDs (Figs. 5C and S10). Note that 2, 10, 20 and 50 % were also tested, and the effect on the TRIDeR/TRIDaR threshold initiation values are described in Text S1. TRIDeR initiation times were found to be mostly instantaneous at each exposure concentration with a value of 17, 16 and 17 s, for the exposure concentrations of  $1 \times 10^{-7}$ ,  $5 \times 10^{-7}$  and  $1 \times 10^{-6}$

M Co, respectively. Over the first few moments of exposure (36 s), 23.5 %, 28.6 % and 24.9 % of untargeted meta-metabolomic features with a bell-shaped time-response trend were impacted in biofilms exposed to  $1 \times 10^{-7}$ ,  $5 \times 10^{-7}$  and  $1 \times 10^{-6}$  M, respectively (Fig. 5A, B and Table 2). The first untargeted meta-metabolomic feature in the control group was affected after 64 min (Fig. 5 and Table 2).

More than half (58.1 %) of untargeted meta-metabolomic features with a biphasic trend and 4.7 % with a monotonic trend were impacted within the TRIDeR for biofilms exposed to  $1 \times 10^{-7}$  M (Table 2). Similar results were observed for biofilms exposed to  $5 \times 10^{-7}$  and  $1 \times 10^{-6}$  M, with 72.3 % and 64.2 % of untargeted meta-metabolomic features with a biphasic trend, respectively, and 6.0 % and 5.6 % with a monotonic trend also impacted within the TRIDeR (Table 2). The TRIDaR initiation times appeared after one day at each exposure concentration: 1.61 d, 1.44 d and 1.74 d, respectively (Fig. 5A and Table 2). The ECDF profiles were similar between exposure concentrations ( $1 \times 10^{-7}$ ,  $5 \times 10^{-7}$  and  $1 \times 10^{-6}$  M groups) and different from those of the control group (Fig. 5A and B). The proportions of untargeted meta-metabolomic features with biphasic dose-response trends were significantly greater in TRIDeR than in TRIDaR (Pearson's test,  $p < 0.001$ ; Table 2). Conversely, the proportions of untargeted meta-metabolomic features with monotonic dose-response trends were significantly greater in TRIDaR than in TRIDeR (Pearson's  $\chi^2$  test,  $p < 0.001$ ; Table 2).

#### 3.5. Comparison of the composition change dynamics between the meta-metabolome and microbial communities

The global metabolite content changes (expressed as a % of the total composition change trajectories over 28 days) observed in the meta-metabolome occurred more rapidly than those observed in the prokaryotic and eukaryotic community compositions, regardless of Co exposure concentrations (Fig. 6A–D). The early change (1 h) in the meta-metabolome due to Co exposure was 20.8, 21.8 and 23.7 % (of the total change observed during the 28 days) compared with the control biofilms exposed to  $1 \times 10^{-7}$ ,  $5 \times 10^{-7}$  and  $1 \times 10^{-6}$  M, respectively. At the same time point, the dynamics of change in the prokaryotic community were 11.1, 11.6 and 14.3 %, respectively, and 12.6, 12.5 and 12.4 %, respectively, in the eukaryotic community. In the control group, the dynamics of composition change were faster in the eukaryotic community than in the prokaryotic community (Fig. 6A). Similar rates of change were observed in biofilm communities exposed to  $1 \times 10^{-7}$  M,

**Table 2**  
Calculated TRIDeR and TRIDaR for each Co exposure concentration group.

| Exposure concentration | Time range  | TRIDeR (day) |                 | TRIDaR (day) |        | Pearson's $\chi^2$ test |                                   |                         |                         |
|------------------------|-------------|--------------|-----------------|--------------|--------|-------------------------|-----------------------------------|-------------------------|-------------------------|
|                        |             | Trend        | Number          | %            | Number | %                       | $\chi^2$                          | d.f.                    | p-Value                 |
| $1 \times 10^{-7}$ M   | Time range  |              | 0.000165 – 1.61 |              | 1.61 – |                         | With Yates' continuity correction |                         |                         |
|                        | Bell-shaped |              | 330             | 68.0         | 155    | 32.0                    |                                   |                         |                         |
|                        | U-shaped    |              | 2               | 2.3          | 84     | 97.7                    |                                   |                         |                         |
|                        | Increasing  |              | 70              | 4.8          | 1383   | 95.2                    |                                   |                         |                         |
|                        | Decreasing  |              | 0               | 0.0          | 49     | 100.0                   |                                   |                         |                         |
|                        | Biphasic    |              | 332             | 58.1         | 239    | 41.9                    | 752.0173                          | 1                       | $1.46 \times 10^{-165}$ |
|                        | Monotonic   |              | 70              | 4.7          | 1432   | 95.3                    |                                   |                         |                         |
|                        | Time range  |              | 0.000188 – 0.94 |              | 0.94 – |                         | With Yates' continuity correction |                         |                         |
|                        | Bell-shaped |              | 365             | 79.3         | 104    | 20.7                    |                                   |                         |                         |
|                        | U-shaped    |              | 2               | 6.0          | 48     | 94.0                    |                                   |                         |                         |
| Increasing             |             | 49           | 6.3             | 1249         | 93.7   |                         |                                   |                         |                         |
| Decreasing             |             | 0            | 0.0             | 65           | 100.0  |                         |                                   |                         |                         |
| Biphasic               |             | 367          | 70.7            | 152          | 29.3   | 979.5104                | 1                                 | $5.11 \times 10^{-215}$ |                         |
| Monotonic              |             | 49           | 3.6             | 1314         | 96.4   |                         |                                   |                         |                         |
| $5 \times 10^{-7}$ M   | Time range  |              | 0.000206 – 1.74 |              | 1.74 – |                         | With Yates' continuity correction |                         |                         |
|                        | Bell-shaped |              | 312             | 71.2         | 126    | 28.8                    |                                   |                         |                         |
|                        | U-shaped    |              | 7               | 11.9         | 52     | 88.1                    |                                   |                         |                         |
|                        | Increasing  |              | 78              | 5.8          | 1263   | 94.2                    |                                   |                         |                         |
|                        | Decreasing  |              | 0               | 0.0          | 58     | 100.0                   |                                   |                         |                         |
|                        | Biphasic    |              | 319             | 64.2         | 178    | 35.8                    | 757.4193                          | 1                       | $9.78 \times 10^{-167}$ |
|                        | Monotonic   |              | 78              | 5.6          | 1321   | 94.4                    |                                   |                         |                         |

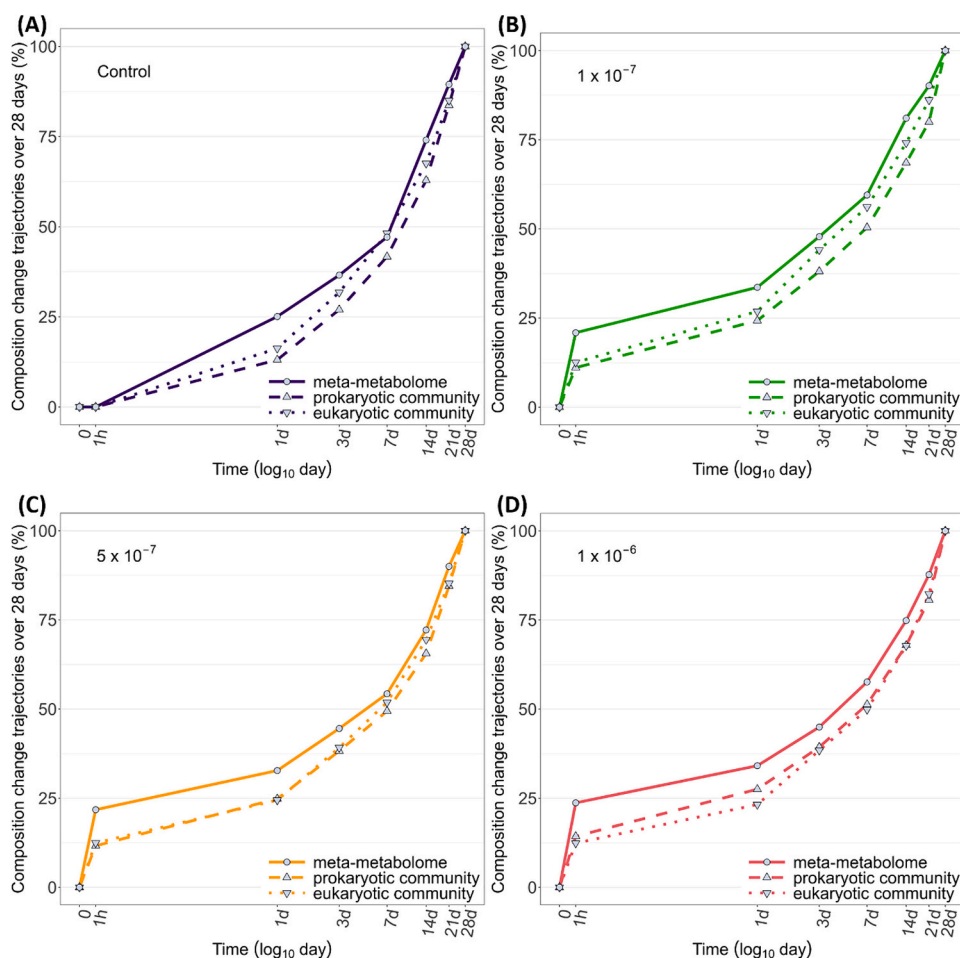


**Fig. 6.** Omics dynamics based on dissimilarities between biofilm meta-metabolomes (Fig. S11A), prokaryotic (Fig. S11B) and eukaryotic (Fig. S11C) communities as a function of Co concentration and exposure time. Composition change trajectories in meta-metabolome (solid line), prokaryotic community (dashed line) and eukaryotic community (dotted line) expressed as percentages of the total trajectory achieved at hour 1, days 1, 3, 7, 14, 21 and 28; (A) for biofilms of control group, (B) for biofilms exposed to  $1 \times 10^{-7}$  M Co, (C) for biofilms exposed to  $5 \times 10^{-7}$  M Co and (D) for biofilms exposed to  $1 \times 10^{-6}$  M Co.

where the dynamics of change were also faster in the 18S-derived community than in the 16S-derived community (Fig. 6B). However, for biofilms exposed to  $1 \times 10^{-6}$  M, the prokaryotic community was impacted more rapidly than the eukaryotic community (Fig. 6D). This transition in change dynamics was gradual, since for biofilms exposed to  $5 \times 10^{-7}$  M, the change dynamics of the two communities were similar up to day 3, with less difference thereafter compared to the control and  $1 \times 10^{-7}$  M Co exposure groups (Fig. 6C).

## 4. Discussion

### 4.1. Concentrations and exposure time to Co induce change in biofilm structure

Cobalt accumulation in biofilms was quantifiable as early as 1 h after exposure (Figs. 1, S2 and Table S2). As with other metals such as Cu, Zn or Ni (Meylan et al., 2003; Laderriere et al., 2020), a correlation between free  $\text{Co}^{2+}$  ion concentrations and intracellular Co was observed (Fig. S2). This bioaccumulation reflects the bioavailability of Co to biofilms, and therefore its potential toxic effects (McGeer et al., 2004).

Control biofilms had specific temporal dynamics over time. An initial increase in biomass was observed during the first week, followed by a gradual decrease until day 21, and an increase again on day 28 (Fig. 2A). The increase in chlorophyll *a* content over the 28-d experiment appeared to be closely linked to that of diatom density (Fig. 2B) consistent with their dominance in relative abundance of the eukaryotic community

(Fig. S4B). A linear regression analysis between the total diatom abundance and chlorophyll *a* content showed a significant positive correlation relationship (Patil and Anil, 2005). An overall change in diversity compared with the initial biofilms was observed over time (without taking into account the exposure concentration factor) for the prokaryotic community after 7 d and after 1 d for the eukaryotic community. These changes therefore appear to be initiated naturally by environmental factors. In fact, the experiment took place in autumn, and water temperatures and sunshine decreased progressively throughout the month of exposure (Table S1). Indeed, after a fall biomass peak, a decrease in specific richness can be observed in river biofilms (Lyautey et al., 2005; Morin et al., 2008b). These observations are also supported by the progressive decrease of alpha diversity indices within the control group, *i.e.* in richness (Fig. S3A), evenness (Fig. S3B) and Shannon (Fig. S3C) for prokaryotes and in richness (Fig. S5A) for eukaryotes.

The structure of biofilms chronically exposed to Co was both rapidly and lastingly affected. With regard to traditional biological monitoring parameters, the biomass of biofilms exposed to  $1 \times 10^{-6}$  M Co began to decrease significantly compared with that of the control group after two weeks of exposure, as did chlorophyll *a* content (Fig. 2A, B and Table S4). These results were in line with those observed following exposures to other metals (Massieux et al., 2004). Surprisingly, the diversity of biofilm communities was rapidly affected by exposure to Co. As early as 1 h after exposure, the communities of prokaryotes exposed to  $5 \times 10^{-7}$  and  $1 \times 10^{-6}$  Co were lower than those of the control group. However, after 1 d of exposure, these differences were no longer

detected. As observed for traditional parameters (biomass and chlorophyll *a* content), prokaryotic and eukaryotic communities were significantly and durably impacted by Co after 14 days of exposure (Figs. 3, S4, S6, Tables S5, S6 and S7). This is in line with the effects of metals on microbial community structures in biofilms. After 21 days of exposure to Ag, structures of bacterial and algal communities were both impacted by exposure conditions (Gil-Allué et al., 2018).

In control biofilms, the eukaryotic community changes more rapidly than the prokaryotic community (Fig. 6A). This is also observed in biofilms exposed to  $1 \times 10^{-7}$  M Co (Fig. 6B). On the other hand, Co seems to influence these dynamics of community changes and succession. In biofilms exposed to  $5 \times 10^{-7}$  M Co, both communities had similar change dynamics on microbial diversity for up to 3 days of exposure (Fig. 6C). This effect was even greater in biofilms exposed to  $1 \times 10^{-6}$  M Co, where the change dynamics proved to be faster for the prokaryotic than the eukaryotic community in terms of taxa occurrence (Fig. 6D). Cobalt would therefore have a faster adverse effect on prokaryotic communities, very likely by inducing the rapid disappearance of the most sensitive taxa.

#### 4.2. Changes in the meta-metabolome are faster than those observed in prokaryotic and eukaryotic community compositions

The comparison of variations at different levels of biological response through different omic approaches (Fig. 6) underlined the value of performing first metabolite extraction prior to DNA extraction on the same sample (Duperron et al., 2023) as applied here for ecotoxicological investigations. Indeed, the three parameters studied (metabolites, 16S and 18S ASVs) came from the same samples, and provided a good representation of the response of microbial communities to contamination on individualized biofilm samples. As emphasized recently, such combination of omics approaches is a new direction to take in environmental risk assessment, and particularly in microbial ecotoxicology (Hellal et al., 2023).

As for the changes observed in biofilm prokaryotic and eukaryotic community structures, the meta-metabolome was rapidly impacted (after 1 h) by Co (Table S8). Then, on days 1, 3 and 7, the meta-metabolomic fingerprint no longer differed between exposed biofilms and those in the control group. This was followed by a more lasting impact from 14 days of exposure to the end of the experiment (Fig. S7). The metabolomic fingerprints of two freshwater microalgae exposed to Cd and Pb were also different from the control group after 2 weeks (Nanda et al., 2021). In a soil, in which the prokaryote community was exposed for 40 days to trinitrotoluene, cyclotrimethylene trinitramine and cyclotetramethylene tetranitramine (alone or in mixtures), the meta-metabolomic fingerprints were also different between exposure groups (Yang et al., 2021), underlining the fact of the lasting effects of stress on the chemical signature of microbial communities.

Cobalt concentrations, exposure time and natural community succession led to progressive changes in the prokaryotic and eukaryotic communities and meta-metabolome of the biofilms. However, on the basis of the percentages of overall change over 28 days deduced from MOTA, the change in the meta-metabolome appeared the most rapid (Fig. 6). Indeed, when comparing the dynamics of change in both control and exposed biofilms, the meta-metabolome changed more rapidly at each time point than the microbial community structure. Within 1 h of exposure, 20.9, 21.8 and 23.7 % of the total meta-metabolome variation had already occurred for biofilms exposed to  $1 \times 10^{-7}$ ,  $5 \times 10^{-7}$  and  $1 \times 10^{-6}$  M Co respectively, compared to the variation of 11.1, 11.6 and 14.3 % for the prokaryotic communities and of 12.6, 12.5 and 12.4 % for the eukaryotic communities (Fig. 6). River biofilms exposed to erythromycin and silver nanoparticles had also showed a change in their meta-metabolome, while prokaryotic community diversity appeared unaffected after 6 and 12 weeks of exposure, respectively (Pu et al., 2021; Yang et al., 2023).

These observations support the view that the (meta-)metabolomic

fingerprint constitutes an instantaneous illustration of the molecular response of organisms in their environment (see Section 4.4). Also, this metabolite fingerprint, which reflects the physiological status of biological systems, appears here even more sensitive than the specific response at the level of the composition of microbial community (see Section 4.3).

#### 4.3. CRIDeR and CRIDaR remain relevant even in a context of changing and “tolerant” communities

The interpretation of trends of dose-response models of untargeted meta-metabolomic features and the identification of CRIDeR and CRIDaR may provide fundamental information on the level of biofilm responses to a stress (Colas et al., 2023). One can expect that these CRIDeR and CRIDaR would be impacted by community changes over time and the appearance of tolerant and resistant species, leading to an increase in their tolerance threshold.

However, the determination of the different CRIDeRs observed at the different time point suggested that defense responses were initiated as soon as the most sensitive microorganisms of the biofilms are first disturbed by an addition of Co in the exposure media. Indeed, the CRIDeRs calculated throughout the experiment had similar initiation threshold values of  $1.41 \pm 0.77 \times 10^{-10}$  M of  $\text{Co}^{2+}$  added in the exposure medium (Table 1). At  $\text{Co}^{2+}$  concentrations above background concentrations ( $1.36 \pm 0.85 \times 10^{-9}$  M  $\text{Co}^{2+}$ ), the metabolic processes of biofilms reacted and appeared to set up molecular defense responses in order to manage Co uptake (Figs. 1, S2 and Table S2). These defense responses took place at lower concentrations than those previously observed in static microcosms (Colas et al., 2023). It is well known that contaminants can impact the (meta-)metabolome of biological systems. At  $4.3 \times 10^{-10}$  M of diuron, biofilm meta-metabolomic fingerprint also began to be impacted as determined via  $\text{BMD}_{-1SD}$  calculation on DRomics (Creusot et al., 2022).

The CRIDeRs of the microbial communities were stable despite a change in taxonomic structure induced by the Co exposure time, which is most likely due to the influence of external environmental factors in addition to the effects induced by Co concentrations (Figs. 3, 4, S4, S6, Tables 1, S5, S6 and S7). After 28 days of exposure to Co, the biofilm communities have probably been able to acclimatize to this disturbance, and be characterized by the presence of so-called tolerant species. An increase in the relative abundance of previously reported as potential metal-tolerant diatom species (Fig. S6 and Table S7), such as *Eolimna minima*, *Fragilaria capucina* var. *capucina*, *Fragilaria capucina* var. *vaucheriae*, *Fragilaria crotonensis*, *Gomphonema parvulum* var. *parvulum* f. *parvulum* or *Mayamaea atomus* var. *permitis* was observed on day 28 (Duong et al., 2008; Thili et al., 2011b; Morin et al., 2012). Also, a decrease in microbial species known to be metal-sensitive was also observed with increasing Co concentrations, such as *Cocconeis placentula* var. *lineata*. In a previous study (Colas et al., 2023), Co induced a change in the composition of photosynthetic pigments, with an increase in the proportion of chlorophyll *b* compared with chlorophylls *a* and  $c_1 + c_2$ , possibly indicating the favored presence of green algae. On day 28, the greater presence of Chlorophyceae and Ulvophyceae in eukaryote communities in biofilms exposed to the two highest concentrations would thus confirm the metal resistance of certain green algae (Ivorra et al., 2000; Corcoll et al., 2011).

Despite microbial community changes occurring during the 28 days exposure time series, such as an increase in tolerant species and a decrease in sensitive species, the CRIDeR observed after 1 h or after 28 d present both very similar Co initiation-threshold concentrations at above  $1.55$  and  $0.92 \times 10^{-10}$  M of  $\text{Co}^{2+}$  added in the exposure medium, respectively (Table 1). Trend analyses of the dose-response curves of untargeted meta-metabolomic features therefore seems relevant regardless of exposure time, even in a context of change and succession of prokaryotic and eukaryotic communities. Despite changes in communities (Figs. 3, S3, S4, S5 and S6), the presence of metal-tolerant

species and the disappearance of metal-sensitive species (Table S7), the concentrations at which defensive responses are initiated (Table 1) remain similar over time. Interestingly, defense mechanisms such as superoxide dismutase activity were observed continuously (from 6 h to 21 d) during exposure to ZnO nanoparticles in river biofilms (Hou et al., 2016).

As Co concentrations increased, a CRIDaR was also characterized at each time point with increasingly higher Co initiation-thresholds (Table 1). While biofilms maintained similar CRIDeR initiation thresholds over time (Table 1), the CRIDaR thresholds increased. This could indicate that the tolerance of microbial communities to Co is manifested by greater resistance to concentrations. Molecular damage would thus occur at higher concentrations after 28 days of exposure than after 1 h or 1 day (Fig. S9A, G and Table 1). The  $BMD_{-1SD}$  calculated for chlorophyll *a* content (which is a biomarker of damage to organisms), was well and truly included in the CRIDaR (Fig. 4C). This reinforces the relevance of characterizing CRIDeRs/CRIDaRs based on dose-response curve trends. At the same time, defensive responses are still in place from the smallest increases in Co concentration in the environment (Fig. S9A and G).

Note that the modeling of dose-response curves, from which  $BMDs_{-1SD}$  were calculated, ECDFs constructed and CRIDeRs and CRIDaRs determined, was relying on the number of Co concentrations that were tested and integrated within the model. This number of exposure concentrations could represent a limiting factor in this approach, as the observation of biphasic trends in biomarker responses in ecotoxicology was restricted by the number of concentrations tested in the studies (Colas and Le Faucheur, 2024).

#### 4.4. TRIDeR and TRIDaR highlight rapid responses to Co exposure

As expected, the calculation of TRIDeR and TRIDaR following the same approach as previously developed for CRIDeR/CRIDaR and considering the exposure time factor instead of concentrations, is feasible and provides relevant findings. Indeed, whatever the Co concentration tested, exposed biofilms exhibited a TRIDeR initiation threshold of above 17 s (Fig. 5 and Table 2). However, bioaccumulation data (Fig. S2 and Table S2) suggested that biofilms began to bioaccumulate Co as early as 1 h after exposure. The quick-acting effect of TRIDeR initiation was observed here after only seconds, as expected with the almost immediate metal internalization and potential cellular impact. In fact, the untargeted meta-metabolomic features appear almost instantaneously in each of the concentrations tested, suggesting the occurrence of immediate metabolic effects resultant of intracellular Co increase. Indeed, after 1 min of exposure, 28.0, 31.1 and 28.1 % of the whole metabolite feature set were altered in comparison to control (all with a bell-shaped dose-response trend), after exposure to  $1 \times 10^{-7}$ ,  $5 \times 10^{-7}$  or  $1 \times 10^{-6}$  M Co, respectively (Fig. 5 and Table 2). After 1 h of exposure, these levels of impacted untargeted meta-metabolomic features rose by 60.9, 72.5 and 63.0 %, respectively (Fig. 5 and Table 2). In contrast, the first untargeted meta-metabolomic features were impacted only after 1 h in control biofilms (Fig. 5 and Table 2). This shows that, at the metabolome level, biofilms are extremely sensitive to perturbations in the aquatic environment, given their continuous, equilibrium interaction with it. Interestingly, similar rapid responses in the order of tens of seconds were also observed in biofilms exposed to diuron (Creusot et al., 2022). Another study also showed the almost instantaneous (< 1 min) effects of this contaminant on river biofilms and on their photosynthetic activity (Morin et al., 2018), demonstrating the immediate responsiveness of biofilms to such chemical disturbances in its environment. Microalgae also responded rapidly to metal exposure, producing phytochelatins after 15 min of exposure to Cu, Cd and Pb (Morelli and Scarano, 2001, 2004). In river biofilm exposed to ZnO nanoparticles, defense responses were initiated after 6 h of exposure with an increase in the activity of catalase and superoxide dismutase as a function of contaminant concentration (Hou et al., 2016).

The ECDFs of the untargeted meta-metabolomic features of exposed

biofilms showed similar temporal profiles at each Co concentration, being largely distinguishable from the slow variations observed in control biofilms (Fig. 5). The TRIDaR initiation thresholds were similar for biofilms exposed to  $1 \times 10^{-7}$ ,  $5 \times 10^{-7}$  and  $1 \times 10^{-6}$  M Co with an exposure time of  $1.4 \pm 0.4$  d. According to the literature, rapid damage effects were also observed on wastewater microbial communities after 5 h of exposure to graphene oxide, with a significant decrease in metabolic activity that also appears to be proportional to increasing contaminant concentrations (Ahmed and Rodrigues, 2013). Taken together, one can deduce that the microbial biofilms response to acute toxicant exposure comprises both defense and damage mechanisms that are mobilized and inducible within tens of seconds and several hours, respectively. However, in order to strengthen the relevance of the TRIDeR/TRIDaR approach, a more in-depth analysis of the literature would enable us to make a definitive statement on the time-response trends of known defense and damage biomarkers.

## 5. Conclusion

Exposure to Co for 28 days had various effects on the structure of river biofilms. A decrease in biomass, chlorophyll *a* content and a change in the composition and diversity of prokaryotic and eukaryotic communities were observed. Within diatom populations, an increase in the relative abundance of metal-resistant diatom species as well as a decrease in the relative abundance of metal-sensitive diatom species were also observed.

The use of the whole meta-metabolomic fingerprint of biofilms appears to be a promising biological compartment to be studied for environmental risk assessment, providing additional and complementary information to traditional monitoring parameters and the information deduced solely from few annotated or targeted metabolites.

CRIDeR and CRIDaR characterizations appear consistent even in the long time-series situation where community dynamics are influenced by both the Co concentrations and the exposure time. In particular, it was observed that potentially tolerant and resistant communities present defense responses similar to those of newly exposed biofilms at similar Co concentrations. Interestingly, these microbial communities, which have probably become tolerant following continuous and long-term exposure, are more resistant to the harmful effects caused by Co.

The TRIDeR and TRIDaR determinations reinforce the fact that the microbial biofilm meta-metabolome is a biological component in close and continuous interaction with the external environment, making it possible to appreciate the rapid rate at which Co affects riparian microbial communities. This study also highlighted the complementarity of multi-omics approaches to better understand the factors driving the responses of a community to stress. Above all, these results confirm the usefulness of analyzing all untargeted metabolomic features with a holistic approach without being restricted by their annotation (and putative functions retrieved from previous observation), proposing CRIDeR/CRIDaR and TRIDeR/TRIDaR as additional new tools for ecotoxicology and microbial ecology studies.

## Funding

This research was funded by the Research Partnership Chair E2S-UPPA-TotalEnergies-Rio Tinto (ANR-16-IDEX-0002).

## CRedit authorship contribution statement

**Simon Colas:** Writing – review & editing, Writing – original draft, Visualization, Validation, Software, Methodology, Investigation, Formal analysis, Data curation, Conceptualization. **Benjamin Marie:** Writing – review & editing, Visualization, Software, Investigation, Formal analysis, Data curation. **Soizic Morin:** Writing – review & editing, Visualization, Investigation, Formal analysis. **Mathieu Milhe-Poutignon:** Investigation, Formal analysis. **Pierre Foucault:** Writing – review &

editing, Software. **Siann Chalvin**: Investigation, Formal analysis. **Clémentine Gelber**: Writing – review & editing, Resources, Project administration. **Patrick Baldoni-Andrey**: Writing – review & editing, Resources, Funding acquisition. **Nicholas Gurieff**: Writing – review & editing, Resources, Funding acquisition. **Claude Fortin**: Writing – review & editing, Supervision. **Séverine Le Faucheur**: Writing – review & editing, Writing – original draft, Validation, Supervision, Resources, Project administration, Investigation, Funding acquisition, Conceptualization.

### Declaration of competing interest

The authors declare that they have no known competing financial interests or personal relationships that could have appeared to influence the work reported in this paper.

### Data availability

Data will be made available on request.

### Acknowledgments

We would like to thank the members of the Environment & Sustainable Development Team, at Pôle d'Etudes et de Recherche de Lacq (PERL) for access to the TotalEnergies facilities for mesocosm exposures and assistance during experimentation. We are grateful to the UMR 7245 MCAM, Muséum National d'Histoire Naturelle, Paris, France, especially the "Cyanobactéries, Cyanotoxines et Environnement" (CCE) team and the Plateau technique de spectrométrie de masse bio-organique (PtSMB) for laboratories and technical facilities for meta-metabolomics analysis. Part of the experiments (amplicon sequencing) were performed at the PGTB (doi:10.15454/1.5572396583599417E12) with the assistance of Zachary Allouche and Zoé Delporte. We also thank Claire Gassie (Université de Pau et des Pays de l'Adour, E2S-UPPA, CNRS, IPREM, Pau, France) for her help in characterization of prokaryotic and eukaryotic communities and Catherine Chamorro (Université de Pau et des Pays de l'Adour, E2S-UPPA, CNRS, IPREM, Pau, France) for his help in the graphic representation of the study area. Special thanks to Scott Hepditch (Institut National de la Recherche Scientifique – Eau Terre Environnement, Québec, Canada) for his language assistance.

### Appendix A. Supplementary data

Detailed results on the physicochemical parameters of the exposure media; biofilm metal contents; Co effects on biofilm biomass, chlorophyll *a* content, diatom mortality and density; alpha- and beta-diversity indexes and compositions of prokaryotic and eukaryotic communities; untargeted and annotated meta-metabolomic fingerprints, T-SNE molecular network, BMDs<sub>-1SD</sub> and BMTs<sub>-1SD</sub> values; determination of CRIDeR/CRIDaR and TRIDeR/TRIDaR initiation thresholds, dissimilarity between biofilm meta-metabolomes, prokaryotic and eukaryotic communities are presented in Supplementary material. Supplementary data to this article can be found online at <https://doi.org/10.1016/j.scitotenv.2024.171851>.

### References

Afgan, E., Baker, D., Batut, B., van den Beek, M., Bouvier, D., Čech, M., Chilton, J., Clements, D., Coraor, N., Grüning, B.A., Guerler, A., Hillman-Jackson, J., Hiltemann, S., Jalili, V., Rasche, H., Soranzo, N., Goecks, J., Taylor, J., Nekrutenko, A., Blankenberg, D., 2018. The galaxy platform for accessible, reproducible and collaborative biomedical analyses: 2018 update. *Nucleic Acids Res.* 46, W537–W544. <https://doi.org/10.1093/nar/gky379>.

Ahmed, F., Rodrigues, D.F., 2013. Investigation of acute effects of graphene oxide on wastewater microbial community: a case study. *J. Hazard. Mater.* 256–257, 33–39. <https://doi.org/10.1016/j.jhazmat.2013.03.064>.

Arbizu, P.M., 2022. pairwiseAdonis: Pairwise Multilevel Comparison Using Adonis.

Barranguet, C., Greijdanus, M., Sinke, J.J., Admiraal, W., 2003. Copper-induced modifications of the modifications of the trophic relations in riverine algal-bacterial biofilms. *Environ. Toxicol. Chem.* 22, 1340–1349. <https://doi.org/10.1002/etc.5620220622>.

Barrio-Parra, F., Elfo, J., De Miguel, E., García-González, J.E., Izquierdo, M., Álvarez, R., 2018. Environmental risk assessment of cobalt and manganese from industrial sources in an estuarine system. *Environ. Geochem. Health* 40, 737–748. <https://doi.org/10.1007/s10653-017-0020-9>.

Bártová, K., Hilscherová, K., Babica, P., Maršálek, B., Bláha, L., 2011. Effects of microcystin and complex cyanobacterial samples on the growth and oxidative stress parameters in green alga *Pseudokirchneriella subcapitata* and comparison with the model oxidative stressor-herbicide paraquat. *Environ. Toxicol.* 26, 641–648. <https://doi.org/10.1002/tox.20601>.

Bonet, B., Corcoll, N., Acuña, V., Sigg, L., Behra, R., Guasch, H., 2013. Seasonal changes in antioxidant enzyme activities of freshwater biofilms in a metal polluted Mediterranean stream. *Sci. Total Environ.* 444, 60–72. <https://doi.org/10.1016/j.scitotenv.2012.11.036>.

Booth, S.C., Workentine, M.L., Weljie, A.M., Turner, R.J., 2011. Metabolomics and its application to studying metal toxicity. *Metabolomics* 3, 1142. <https://doi.org/10.1039/c1mt00070e>.

Bradley, I.M., Pinto, A.J., Guest, J.S., 2016. Design and evaluation of Illumina MiSeq-compatible, 18S rRNA gene-specific primers for improved characterization of mixed phototrophic communities. *Appl. Environ. Microbiol.* 82, 5878–5891. <https://doi.org/10.1128/AEM.01630-16>.

Bryan, S.E., Tipping, E., Hamilton-Taylor, J., 2002. Comparison of measured and modelled copper binding by natural organic matter in freshwaters. *Comp. Biochem. Physiol., Part C: Toxicol. Pharmacol.* 133, 37–49. [https://doi.org/10.1016/S1532-0456\(02\)00083-2](https://doi.org/10.1016/S1532-0456(02)00083-2).

Cailleaud, K., Bassères, A., Gelber, C., Postma, J.F., Ter Schure, A.T., Leonards, P.E.G., Redman, A.D., Whale, G.F., Spence, M.J., Hjort, M., 2019. Investigating predictive tools for refinery effluent hazard assessment using stream mesocosms. *Environ. Toxicol. Chem.* 38, 650–659. <https://doi.org/10.1002/etc.4338>.

Çelekli, A., Kapt, M., Bozkurt, H., 2013. Effect of cadmium on biomass, pigmentation, malondialdehyde, and proline of *Scenedesmus quadricauda* var. *longispina*. *Bull. Environ. Contam. Toxicol.* 91, 571–576. <https://doi.org/10.1007/s00128-013-1100-x>.

Cheng, J., Qiu, H., Chang, Z., Jiang, Z., Yin, W., 2016. The effect of cadmium on the growth and antioxidant response for freshwater algae *Chlorella vulgaris*. *SpringerPlus* 5, 1290. <https://doi.org/10.1186/s40064-016-2963-1>.

Colas, S., Le Faucheur, S., 2024. How do biomarkers dance? Specific moves of defense and damage biomarkers for biological interpretation of dose-response model trends. *J. Hazard. Mater.* 465, 133180. <https://doi.org/10.1016/j.jhazmat.2023.133180>.

Colas, S., Duval, C., Marie, B., 2020. Toxicity, transfer and depuration of anatoxin-a (cyanobacterial neurotoxin) in medaka fish exposed by single-dose gavage. *Aquat. Toxicol.* 222, 105422. <https://doi.org/10.1016/j.aquatox.2020.105422>.

Colas, S., Marie, B., Milhe-Poutingon, M., Lot, M.-C., Boulemant, A., Fortin, C., Le Faucheur, S., 2023. Meta-metabolomic responses of river biofilms to cobalt exposure and use of dose-response model trends as an indicator of effects. *BioRxiv*. <https://doi.org/10.1101/2023.06.19.545533>.

Corcoll, N., Bonet, B., Leira, M., Guasch, H., 2011. Chl-a fluorescence parameters as biomarkers of metal toxicity in fluvial biofilms: an experimental study. *Hydrobiologia* 673, 119–136. <https://doi.org/10.1007/s10750-011-0763-8>.

Coste, M., Rosebery, J., 2011. Guide iconographique pour la mise en oeuvre de l'Indice Biologique Diatomée 2007, Action14: Développement et optimisation des méthodes de bioindication pour les cours d'eau. Cestas Gazinet, Cemagref groupement de Bordeaux, p. 241.

Creusot, N., Chaumet, B., Eon, M., Mazzella, N., Moreira, A., Morin, S., 2022. Metabolomics insight into the influence of environmental factors in responses of freshwater biofilms to the model herbicide diuron. *Environ. Sci. Pollut. Res.* 29, 29332–29347. <https://doi.org/10.1007/s11356-021-17072-7>.

da Silva, R.R., Dorrestein, P.C., Quinn, R.A., 2015. Illuminating the dark matter in metabolomics. *Proc. Natl. Acad. Sci.* 112, 12549–12550. <https://doi.org/10.1073/pnas.151687811>.

Dias, D., Jones, O., Beale, D., Boughton, B., Benheim, D., Kouremenos, K., Wolfender, J.-L., Wishart, D., 2016. Current and future perspectives on the structural identification of small molecules in biological systems. *Metabolites* 6, 46. <https://doi.org/10.3390/metabo6040046>.

Doose, C., Fadhlaoui, M., Morin, S., Fortin, C., 2021. Thorium exposure drives fatty acid and metal transfer from biofilms to the grazer *Lymnaea* sp. *Environ. Toxicol. Chem.* 40, 2220–2228. <https://doi.org/10.1002/etc.5067>.

Duong, T.T., Morin, S., Herlory, O., Feurtet-Mazel, A., Coste, M., Boudou, A., 2008. Seasonal effects of cadmium accumulation in periphytic diatom communities of freshwater biofilms. *Aquat. Toxicol.* 90, 19–28. <https://doi.org/10.1016/j.aquatox.2008.07.012>.

Duong, T.T., Morin, S., Coste, M., Herlory, O., Feurtet-Mazel, A., Boudou, A., 2010. Experimental toxicity and bioaccumulation of cadmium in freshwater periphytic diatoms in relation with biofilm maturity. *Sci. Total Environ.* 408, 552–562. <https://doi.org/10.1016/j.scitotenv.2009.10.015>.

Duperron, S., Foucault, P., Duval, C., Goto, M., Gallet, A., Colas, S., Marie, B., 2023. Multi-omics analyses from a single sample: prior metabolite extraction does not alter the 16S rRNA-based characterization of prokaryotic community in a diversity of sample types. *FEMS Microbiol. Lett.* 370, fnad125. <https://doi.org/10.1093/fems/lnad125>.

Dutta, A., Mandal, A., Chanda, P., Misra, S., Mukherjee, J., Das, R., 2022. Biosorption of cadmium and cobalt by intertidal multicomponent biofilms. *Mar. Pollut. Bull.* 185, 114318. <https://doi.org/10.1016/j.marpolbul.2022.114318>.

- El-Sheekh, M.M., El-Naggar, A.H., Osman, M.E.H., El-Mazaly, E., 2003. Effect of cobalt on growth, pigments and the photosynthetic electron transport in *Monoraphidium minutum* and *Nitzschia perminuta*. *Braz. J. Plant Physiol.* 15, 159–166. <https://doi.org/10.1590/S1677-0420200300030005>.
- European Chemicals Agency, 2023. Cobalt - Registration Dossier - ECHA [WWW Document]. <https://echa.europa.eu/registration-dossier/-/registered-dossier/15506/6/1> (accessed 9.19.23).
- Fawzy, M.A., Hifney, A.F., Adam, M.S., Al-Badaani, A.A., 2020. Biosorption of cobalt and its effect on growth and metabolites of *Synechocystis pevalekii* and *Scenedesmus bernardii*: isothermal analysis. *Environmental Technology & Innovation* 19, 100953. <https://doi.org/10.1016/j.eti.2020.100953>.
- Foucault, P., Gallet, A., Duval, C., Marie, B., Duperron, S., 2022. Gut microbiota and holobiont metabolome composition of the medaka fish (*Oryzias latipes*) are affected by a short exposure to the cyanobacterium *Microcystis aeruginosa*. *Aquat. Toxicol.* 253, 106329. <https://doi.org/10.1016/j.aquatox.2022.106329>.
- Gauthier, L., Tison-Rosebery, J., Morin, S., Mazzella, N., 2020. Metabolome response to anthropogenic contamination on microalgae: a review. *Metabolomics* 16, 8. <https://doi.org/10.1007/s11306-019-1628-9>.
- Gil-Allué, C., Tlili, A., Schirmer, K., Gessner, M.O., Behra, R., 2018. Gil-Allué, C., Tlili, a., Schirmer, K., Gessner, M. O., & Behra, R. (2018). Long-term exposure to silver nanoparticles affects periphyton community structure and function. *Environmental science: Nano*, 5(6), 1397–1407. *Environment Science: Nano* 5, 1397–1407. <https://doi.org/10.1039/C8EN00132D>.
- Gray, J.E., Eppinger, R.G., 2012. Distribution of Cu, Co, As, and Fe in mine waste, sediment, soil, and water in and around mineral deposits and mines of the Idaho Cobalt Belt, USA. *Appl. Geochem.* 27, 1053–1062. <https://doi.org/10.1016/j.apgeochem.2012.02.001>.
- Hellal, J., Barthelmebs, L., Bérard, A., Cébron, A., Cheloni, G., Colas, S., Cravo-Laureau, C., De Clerck, C., Gallois, N., Hery, M., Martin-Laurent, F., Martins, J., Morin, S., Palacios, C., Pesce, S., Richaume, A., Vuilleumier, S., 2023. Unlocking secrets of microbial ecotoxicology: recent achievements and future challenges. *FEMS Microbiol. Ecol.*, fiad102. <https://doi.org/10.1093/femsec/fiad102>.
- Hou, J., You, G., Xu, Y., Wang, C., Wang, P., Miao, L., Dai, S., Lv, B., Yang, Y., 2016. Antioxidant enzyme activities as biomarkers of fluvial biofilm to ZnO NPs ecotoxicity and the integrated biomarker responses (IBR) assessment. *Ecotoxicol. Environ. Saf.* 133, 10–17. <https://doi.org/10.1016/j.ecoenv.2016.06.014>.
- Ivorra, N., Bremer, S., Guasch, H., Kraak, M.H., Admiraal, W., 2000. Differences in the sensitivity of benthic microalgae to Zn and Cd regarding biofilm development and exposure history. *Environmental Toxicology and Chemistry: An International Journal* 19, 1332–1339. <https://doi.org/10.1002/etc.5620190516>.
- Jeffrey, S.W., Humphrey, G.F., 1975. New spectrophotometric equations for determining chlorophylls a, b, c<sub>1</sub> and c<sub>2</sub> in higher plants, algae and natural phytoplankton. *Biochem. Physiol. Pflanz.* 167, 191–194. [https://doi.org/10.1016/S0015-3796\(17\)30778-3](https://doi.org/10.1016/S0015-3796(17)30778-3).
- Karthikeyan, P., Marigoudar, S.R., Nagarajuna, A., Sharma, K.V., 2019. Toxicity assessment of cobalt and selenium on marine diatoms and copepods. *Environmental Chemistry and Ecotoxicology* 1, 36–42. <https://doi.org/10.1016/j.enceo.2019.06.001>.
- Laderrière, V., Paris, L.-E., Fortin, C., 2020. Proton competition and free ion activities drive cadmium, copper, and nickel accumulation in river biofilms in a nordic ecosystem. *Environments* 7, 112. <https://doi.org/10.3390/environments7120112>.
- Larras, F., Billoir, E., Baillard, V., Siberchicot, A., Scholz, S., Wubet, T., Tarkka, M., Schmitt-Jansen, M., Delignette-Muller, M.-L., 2018. DRomics: a turnkey tool to support the use of the dose–response framework for omics data in ecological risk assessment. *Environ. Sci. Technol.* 52, 14461–14468. <https://doi.org/10.1021/acs.est.8b04752>.
- Lavoie, I., Lavoie, M., Fortin, C., 2012b. A mine of information: benthic algal communities as biomonitors of metal contamination from abandoned tailings. *Sci. Total Environ.* 425, 231–241. <https://doi.org/10.1016/j.scitotenv.2012.02.057>.
- Lavoie, M., Fortin, C., Campbell, P.G.C., 2012a. Influence of essential elements on cadmium uptake and toxicity in a unicellular green alga: the protective effect of trace zinc and cobalt concentrations. *Environ. Toxicol. Chem.* 31, 1445–1452. <https://doi.org/10.1002/etc.1855>.
- Le Moigne, D., Demay, J., Reinhardt, A., Bernard, C., Kim Tiam, S., Marie, B., 2021. Dynamics of the metabolome of *Alainostoc* sp. PMC 882.14 in response to light and temperature variations. *Metabolites* 11, 745. <https://doi.org/10.3390/metabo11110745>.
- Li, M., Hu, C., Zhu, Q., Chen, L., Kong, Z., Liu, Z., 2006. Copper and zinc induction of lipid peroxidation and effects on antioxidant enzyme activities in the microalga *Pavlova viridis* (Prymnesiophyceae). *Chemosphere* 62, 565–572. <https://doi.org/10.1016/j.chemosphere.2005.06.029>.
- Li, M., Zhu, Q., Hu, C., Chen, L., Liu, Z., Kong, Z., 2007. Cobalt and manganese stress in the microalga *Pavlova viridis* (Prymnesiophyceae): effects on lipid peroxidation and antioxidant enzymes. *J. Environ. Sci.* 19, 1330–1335. [https://doi.org/10.1016/S1001-0742\(07\)60217-4](https://doi.org/10.1016/S1001-0742(07)60217-4).
- Liu, X., Chen, Q., Ali, N., Zhang, J., Wang, M., Wang, Z., 2019. Single and joint oxidative stress-related toxicity of sediment-associated cadmium and lead on *Bellamyia aeruginosa*. *Environ. Sci. Pollut. Res.* 26, 24695–24706. <https://doi.org/10.1007/s11356-019-05769-9>.
- Lyautey, E., Jackson, C.R., Cayrou, J., Rols, J.L., Garabétian, F., 2005. Lyautey, E., Jackson, C. R., Cayrou, J., Rols, J. L., & Garabétian, F. (2005). Bacterial community succession in natural river biofilm assemblages. *Microbial ecology*, 50, 589–601. *Microb. Ecol.* 50, 589–601. <https://doi.org/10.1007/s00248-005-5032-9>.
- Martens, H., Barg, M., Warren, D., Jah, J.-H., 2002. Microbial production of vitamin B 12. *Appl. Microbiol. Biotechnol.* 58, 275–285. <https://doi.org/10.1007/s00253-001-0902-7>.
- Massieux, B., Boivin, M.E.Y., van den Ende, F.P., Langenskiöld, J., Marvan, P., Barranguet, C., Admiraal, W., Laanbroek, H.J., Zwart, G., 2004. Analysis of structural and physiological profiles to assess the effects of Cu on biofilm microbial communities. *Appl. Environ. Microbiol.* 70, 4512–4521. <https://doi.org/10.1128/AEM.70.8.4512-4521.2004>.
- McGeer, J., Henningsen, G., Lanno, R., Fisher, N., Sappington, K., Drexler, J., Beringer, M., 2004. Issue Paper on the Bioavailability and Bioaccumulation of Metals. *Environmental Protection Agency, U.S.*
- McMurdie, P.J., Holmes, S., 2013. Phyloseq: an R package for reproducible interactive analysis and graphics of microbiome census data. *PLoS One* 8, e61217. <https://doi.org/10.1371/journal.pone.0061217>.
- Meylan, S., Behra, R., Sigg, L., 2003. Accumulation of copper and zinc in periphyton in response to dynamic variations of metal speciation in freshwater. *Environ. Sci. Technol.* 37, 5204–5212. <https://doi.org/10.1021/es034566-f>.
- Morelli, E., Scarano, G., 2001. Synthesis and stability of phytochelutins induced by cadmium and lead in the marine diatom *Phaeodactylum tricornutum*. *Mar. Environ. Res.* 52, 383–395. [https://doi.org/10.1016/S0141-1136\(01\)00093-9](https://doi.org/10.1016/S0141-1136(01)00093-9).
- Morelli, E., Scarano, G., 2004. Copper-induced changes of non-protein thiols and antioxidant enzymes in the marine microalga *Phaeodactylum tricornutum*. *Plant Sci.* 167, 289–296. <https://doi.org/10.1016/j.plantsci.2004.04.001>.
- Morin, Soizic, Duong, T.T., Herlory, O., Feurtet-Mazel, A., Coste, M., 2008a. Cadmium toxicity and dynamic variations in freshwater biofilms. *Arch. Environ. Contam. Toxicol.* 54, 173–186. <https://doi.org/10.1007/s00244-007-9022-4>.
- Morin, S., Duong, T.T., Dabrin, A., Coynel, A., Herlory, O., Baudrimont, M., Delmas, F., Durrieu, G., Schäfer, J., Winterton, P., Blanc, G., Coste, M., 2008b. Long-term survey of heavy-metal pollution, biofilm contamination and diatom community structure in the Riou mort watershed, south-West France. *Environ. Pollut.* 151, 532–542. <https://doi.org/10.1016/j.envpol.2007.04.023>.
- Morin, S., Proia, L., Ricart, M., Bonnineau, C., Geislinger, A., Ricciardi, F., Guasch, H., Romaní, A.M., Sabater, S., 2010. Effects of a bactericide on the structure and survival of benthic diatom communities. *Vie et Milieu / Life & Environment* 60, 109–116.
- Morin, S., Cordonier, A., Lavoie, I., Arini, A., Blanco, S., Duong, T.T., Tornés, E., Bonet, B., Corcoll, N., Faggiano, L., Laviale, M., Pères, F., Becares, E., Coste, M., Feurtet-Mazel, A., Fortin, C., Guasch, H., Sabater, S., 2012. Consistency in diatom response to metal-contaminated environments. In: Guasch, H., Ginebreda, A., Geislinger, A. (Eds.), *Emerging and Priority Pollutants in Rivers: The Handbook of Environmental Chemistry*. Springer, Berlin Heidelberg, Berlin, Heidelberg, pp. 117–146. [https://doi.org/10.1007/978-3-642-25722-3\\_5](https://doi.org/10.1007/978-3-642-25722-3_5).
- Morin, S., Lambert, A.S., Rodriguez, E.P., Dabrin, A., Coquery, M., Pesce, S., 2017. Changes in copper toxicity towards diatom communities with experimental warming. *J. Hazard. Mater.* 334, 223–232. <https://doi.org/10.1016/j.jhazmat.2017.04.016>.
- Morin, S., Chaumet, B., Mazzella, N., 2018. A time-dose response model to assess diuron-induced photosynthesis inhibition in freshwater biofilms. *Front. Environ. Sci.* 6, 131. <https://doi.org/10.3389/fenvs.2018.00131>.
- Nanda, M., Jaiswal, K.K., Kumar, V., Verma, M., Vlaskin, M.S., Gururani, P., Kim, H., Alajmi, M.F., Hussain, A., 2021. Bio-remediation capacity for Cd(II) and Pb(II) from the aqueous medium by two novel strains of microalgae and their effect on lipidomics and metabolomics. *Journal of Water Process Engineering* 44, 102404. <https://doi.org/10.1016/j.jwpe.2021.102404>.
- Olguín, E.J., Sánchez-Galván, G., 2012. Heavy metal removal in phytofiltration and phycoremediation: the need to differentiate between bioadsorption and bioaccumulation. *N. Biotechnol.* 30, 3–8. <https://doi.org/10.1016/j.nbt.2012.05.020>.
- Patil, J.S., Anil, A.C., 2005. Biofilm diatom community structure: influence of temporal and substratum variability. *Biofouling* 21, 189–206. <https://doi.org/10.1080/08927010500256757>.
- Peng, B., Li, H., Peng, X.X., 2015. Functional metabolomics: from biomarker discovery to metabolome reprogramming. *Protein Cell* 6, 628–637. <https://doi.org/10.1007/s12328-015-0185-x>.
- Plekhanov, S.E., Chemeris, Y.K., 2003. Early toxic effects of zinc, cobalt, and cadmium on photosynthetic activity of the green alga *Chlorella pyrenoidosa* Chick S-39. *Biology Bulletin of the Russian Academy of Sciences* 30, 6. <https://doi.org/10.1023/A:1025806921291>.
- Pu, Y., Pan, J., Yao, Y., Ngan, W.Y., Yang, Y., Li, M., Habimana, O., 2021. Ecotoxicological effects of erythromycin on a multispecies biofilm model, revealed by metagenomic and metabolomic approaches. *Environ. Pollut.* 276, 116737. <https://doi.org/10.1016/j.envpol.2021.116737>.
- R Core Team, 2021. R: A language and environment for statistical computing.
- Sonmez, M.C., Ozgur, R., Uzilday, B., 2023. Reactive oxygen species: connecting eustress, hormesis, and allostasis in plants. *Plant Stress* 8, 100164. <https://doi.org/10.1016/j.plstress.2023.100164>.
- Stubblefield, W.A., Van Genderen, E., Cardwell, A.S., Hejerrick, D.G., Janssen, C.R., De Schampelaere, K.A.C., 2020. Acute and chronic toxicity of cobalt to freshwater organisms: using a species sensitivity distribution approach to establish international water quality standards. *Environ. Toxicol. Chem.* 39, 799–811. <https://doi.org/10.1002/etc.4662>.
- Thorley, J., Schwarz, C., 2018. ssdtools: an R package to fit species sensitivity distributions. *J. Open Source Softw.* 3, 1082. <https://doi.org/10.21105/joss.01082>.
- Tien, C.J., Wu, W.H., Chuang, T.L., Chen, C.S., 2009. Tien, C. J., Wu, W. H., Chuang, T. L., & Chen, C. S. (2009). Development of river biofilms on artificial substrates and their potential for biomonitoring water quality. *Chemosphere*, 76(9), 1288–1295. *Chemosphere* 76, 1288–1295. <https://doi.org/10.1016/j.chemosphere.2009.06.013>.

- Tipping, E., 2007. Modelling the interactions of hg(II) and methylmercury with humic substances using WHAM/model VI. *Appl. Geochem.* 22, 1624–1635. <https://doi.org/10.1016/j.apgeochem.2007.03.021>.
- Tlili, A., Marechal, M., Montuelle, B., Volat, B., Dorigo, U., Bérard, A., 2011a. Use of the MicroResp™ method to assess pollution-induced community tolerance to metals for lotic biofilms. *Environ. Pollut.* 159, 18–24. <https://doi.org/10.1016/j.envpol.2010.09.033>.
- Tlili, A., Corcoll, N., Bonet, B., Morin, S., Montuelle, B., Bérard, A., Guasch, H., 2011b. In situ spatio-temporal changes in pollution-induced community tolerance to zinc in autotrophic and heterotrophic biofilm communities. *Ecotoxicology* 20, 1823–1839. <https://doi.org/10.1007/s10646-011-0721-2>.
- U.S. Geological Survey, 2010. Mineral Commodity Summaries 2010. U.S. Geological Survey. <https://doi.org/10.3133/mineral2010>.
- U.S. Geological Survey, 2023. Mineral Commodity Summaries 2023. U.S. Geological Survey. <https://doi.org/10.3133/mcs2023>.
- Wang, Y., Qian, P.-Y., 2009. Conservative fragments in bacterial 16S rRNA genes and primer design for 16S ribosomal DNA amplicons in metagenomic studies. *PloS One* 4, e7401. <https://doi.org/10.1371/journal.pone.0007401>.
- Xu, K., Tang, Z., Liu, S., Liao, Z., Xia, H., Liu, L., Wang, Z., Qi, P., 2018. Effects of low concentrations copper on antioxidant responses, DNA damage and genotoxicity in thick shell mussel *Mytilus coruscus*. *Fish Shellfish Immunol.* 82, 77–83. <https://doi.org/10.1016/j.fsi.2018.08.016>.
- Yang, P., Pan, J., Wang, H., Xiaohan, X., Zeling, X., Chen, X., Yang, Y., Sun, H., Li, M., Habimana, O., 2023. Structural, metagenomic and metabolic shifts in multispecies freshwater biofilm models exposed to silver nanoparticles. *J. Environ. Chem. Eng.* 11, 109162. <https://doi.org/10.1016/j.jece.2022.109162>.
- Yang, X., Lai, J., Zhang, Y., Luo, X., Han, M., Zhao, S., 2021. Microbial community structure and metabolome profiling characteristics of soil contaminated by TNT, RDX, and HMX. *Environ. Pollut.* 285, 117478. <https://doi.org/10.1016/j.envpol.2021.117478>.